New age constraints supporting the existence of protracted deformation in the Delamerian Orogen: 40Ar/39Ar geochronology on fabric forming minerals of the Kanmantoo Group metasediments.

Naina Goswami[1]

[1]*Mineral Exploration Cooperative Research Centre, Research School of Earth Sciences, The Australian National University, Canberra ACT 2601, Australia*

Correspondence to: Naina Goswami (u5960582@anu.edu.au)

Abstract. The final assembly of Gondwanaland following Rodinia breakup during the Neoproterozoic-Cambrian period was marked by tectonic mode switch leading to the transformation of a passive margin in the east to an active subduction margin. This period was marked by subduction of the Pacific plate leading to the initiation of the Delamerian Orogeny in South Australia at c. 515 Ma, culminating at c. 490 Ma. Most studies have attempted to constrain the timing of deformation through dating of magmatic intrusions as proxies for deformation, however, relatively few studies strived to date minerals in fabrics that developed during deformation. As opposed to existing age constraints on the timing of cessation of the Delamerian Orogeny at c. 490 Ma, the work presented here identifies new protracted periods of active regional tectonics in the eastern Mt. Lofty Ranges. This was first observed in the underlying Backstairs Passage Formation overlain by the Tapanappa Formation of the Cambrian Kanmantoo Group through ultra-high vacuum 40Ar/39Ar geochronology and 39Ar diffusion experiments conducted on mica separates. It is observed that younger ages up to c. 468 Ma are recorded in the stratigraphically older Backstairs Passage Formation, while the overlying Tapanappa Formation bears no 40Ar/39Ar apparent ages younger than c. 486 Ma. In addition, age data reveals a period of fluid activity at c. 497-493 Ma resulting in micaceous intrusions locally and regionally. The methodology adopted here involves compilation of the age information with microstructural analyses where the age interval of c. 493-487 Ma is interpreted as post peak-metamorphism garnet growth event. This period is likely associated with retrograde metamorphism and is co-eval with Cu-mineralization in the region at c. 492-485 Ma. A second generation of retrogressed biotite growth at the expense of garnet has been identified. Importantly, there are differences in metamorphic grade and timing of deformation between the stratigraphically older the Backstairs Passage Formation and the younger Tapanappa Formation. This can be explained through macroscopic and/or microscopic processes. Two interpretations are proposed here- first involving the lower activation energy of the Backstairs Passage Formation as a measure of argon retentivity, and therefore younger ages, and the second considering proximity of the two formations to the metamorphic core of the belt at Reedy Creek and the effect of dissipated heat affecting record of argon ages in each unit. These newly identified young ages indicate the protracted nature of the Delamerian Orogeny than previously documented.

1 Introduction

Constraining the timing of deformation events in an orogenic system is a complex task and requires a rigorous assessment and complete understanding of the structural controls that have prevailed in the region for the lifespan of the orogenesis. Conventional methods include dating of magmatic intrusions as proxies for timing the deformation phases i.e., dating of pre-, syn- and post- magmatic bodies bracketing the deformation interval. For this purpose, U-Pb geochronometer is one of the most widely applied tools to date a variety of U-rich minerals (zircon, monazite, titanite etc.), where ages are interpreted to reflect the timing of emplacement of an intrusion. Ideally, however, absolute age dating should be undertaken on minerals that define deformation fabrics within an orogen, as a complimentary tool to the bracketing approach of using igneous intrusions. 40Ar/39Ar geochronology on fabric forming minerals has been undertaken in many orogenic settings for this purpose (e.g., Gibson et al., 1992; Burtt et al., 2000; Foden et al., 2002; Rutherford et al., 2006; Forster and Lister, 2009) In this study, we employ 40Ar/39Ar geochronology on micas within schistose rocks and associated mica-bearing veins in order to provide age constraints on the timing of orogenic activity of an orogenic belt in southern Australia, the Delamerian Orogen.

The Delamerian Orogen of South Australia was active during the Late Cambrian-Early Ordovician period (Foden et al., 1999; Foden et al., 2002). It is part of one of the largest known systems of orogenies on Earth, *the Pan- African Orogenies*, which included accretion of numerous microcontinents to form the supercontinent, Gondwanaland (Turner et al., 1996; Rozendaal et al., 1999; Boger and Miller, 2004; Gray et al., 2006). The Delamerian Orogeny deformed and metamorphosed the Neoproterozoic rocks of the Adelaide Superbasin, the basal Normanville Group and the Late-Cambrian rock package of the overlying Kanmantoo Group. These were deposited in an extensional/transpressional setting prior to the Delamerian Orogeny, accompanied with small volumes of mafic magmatism (Foden et al., 1999). The sedimentation of the Kanmantoo Group accumulated over a short period of time during Early- to Mid-Cambrian (~522-514 Ma, Foden et al., 2002; Foden et al., 2006; Mauger et al., 2018; Foden et al., 2020). The culmination of Delamerian Orogeny was followed by extension of the lithospheric mantle concluding with the intrusion of A-types granites, mafics and volcanics (Turner et al., 1996; Foden et al., 1999; Foden et al., 2020).

One of the key regions within the Delamerian Orogen is the Kanmantoo Mine area where the timing of Cu-Au mineralisation, alteration events and associated structural controls are not fully understood. Monazite microprobe Th-U-Pb dating of drill core sample suggested an age of c. 492 Ma for Cu-mineralisation (Wilson, 2009), post-dating the timing of peak metamorphism. Arbon (2011) and Kimpton (2018) suggested the presence of two distinct chlorite alteration events at c. 503 Ma and c. 501 Ma, each associated with a period of distinct mineralisation episode in the area. The specific relationship between mineralisation and other alteration events at the Kanmantoo Mine and adjoining areas, and Delamerian Orogeny structures have not been fully deciphered. Several studies have been undertaken to correlate the timing of events, whether thermal, deformation and/or metamorphic events in the Kanmantoo Mine area to those of Delamerian Orogeny phase(s) (Fanning, 1990; Perkins and Walsh, 1993; Turner et al., 1993; Drexel and Preiss, 1995; Gray and Webb, 1995; Turner et al., 1996; Turner et al., 1998; Foden et al., 1999; Ireland et al., 2002; Jenkins et al., 2002), however no ^{40}Ar/^{39}Ar geochronology work in this region has been undertaken so far.

This study has undertaken direct dating of Delamerian deformation by employing ^{40}Ar/^{39}Ar geochronology and ^{39}Ar diffusion experiments on fabric forming minerals (micas) so as to contribute to our understanding of mineral systems and deformation in the region. These local area constraints can be extended towards understanding of the broader Delamerian Orogen, and thus, can aid in deciphering the nature of orogenesis.

2 Geological setting
2.1 Background

The Delamerian Orogeny initiated after the cessation of the sedimentation in the Kanmantoo trough (Parker, 1986; Jago et al., 2003; Foden et al., 2006), due to major tectonic mode switch from extensional to compressional tectonics (Flöttmann et al., 1998; Foden et al., 2006). The Delamerian Orogeny is characterised by three stages of deformation conventionally recognised as D_1, D_2 and D_3 (Jenkins and Sandiford, 1992; Flöttmann et al., 1998; Jago et al., 2003), and metamorphic grade increasing from chlorite to migmatite zone from west to east (Fig. 1).

The orogenesis commenced during Middle- to Late- Cambrian period as a response to subduction followed by back-arc extension (Turner et al., 1996; Foden et al., 2020). The first craton-ward D_1 thrust event is timed at ~515 Ma (Foden et al., 2006), and maximum age of D_1 deformation event as 502.4±4 Ma constrained through ^{40}Ar/^{39}Ar dating of the muscovite defining the axial planar S_1 fabric of the middle amphibolite metapelite of the Cambrian Kanmantoo Group (Foden et al., 2020). Estimation on the occurrence of D_2 event is bracketed at ~506-500 Ma (Perkins and Walsh, 1993; Foden et al., 2006), and D_3 event to have lasted from ~495-486 Ma (Drexel and Preiss, 1995; Ireland et al., 2002; Foden et al., 2006).
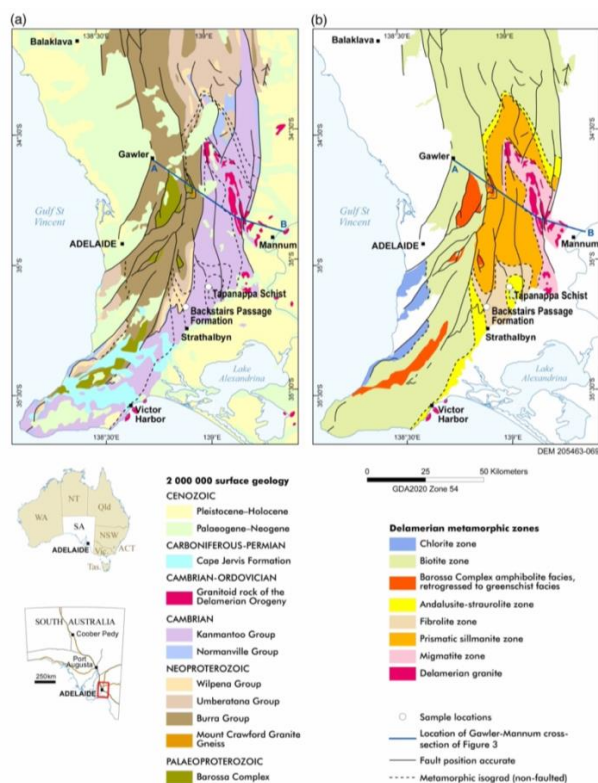
105

Figure 1. Geology of the Mt Lofty Ranges, part of the Delamerian Orogen, showing location of samples analysed in this study (white circles), modified from Reid et al. 2022. (a) 1:2 million scale South Australian state-wide geology dataset. (b) Delamerian metamorphic isograds of the Mt Lofty Ranges (after Offler and Fleming, 1968; Mancktelow, 1990; Dymoke and Sandiford, 1992; Preiss, 1995).

110

The Kanmantoo Group occupies a key position along the Cambrian paleo-pacific margin of southern Gondwana and deposited in a rift basin overlying the Adelaidean stratigraphic units after the lithosphere underwent extension, with sedimentation concluding prior to initiation of the Delamerian Orogeny. The Kanmantoo Group lies disconformably over the Normanville Group forming a 7-8 km thick pile (Jenkins and
115   Sandiford, 1992; Foden et al., 1999). The group consists of metamorphosed clastic turbidites with occasional psammitic beds up to 5 metres in thickness (Haines et al., 2001), and forms a major element of the Adelaide Superbasin (Burtt and Phillips, 2003).

2.2 Kanmantoo Group stratigraphy
120   Stratigraphic sub-divisions of the Kanmantoo Group by Jago et al. (2003) proposed two subgroups (bottom to top), the Keynes Subgroup consisting of the Carrickalinga Head Formation and the Backstairs Passage Formation overlain by the Bollaparudda Subgroup which is host to the Talisker Formation, and base metal deposits of the Tapanappa Formation.

125   Backstairs Passage Formation overlies the basal unit of Kanmantoo Group- Carrickalinga Head Formation and represents a shallow water unit of the Kanmantoo Group. The dominant lithology is laminated to cross-bedded, medium-grained sandstone (Jago et al., 2003). This unit hosts strata bound Pb-Zn sulphides (galena, sphalerite, pyrrhotite).

130   The Paringa Garnet Schist unit of the Tapanappa Formation is a garnetiferous zone within the Kanmantoo Group, well exposed in the Kanmantoo Mine area. The formation predominantly comprises of massive to laminated, fine- to coarse-grained greywacke grading rapidly into thin, light- to dark-grey laminated

siltstones. Within this unit, mineralisation is hosted within the andalusite-garnet schist unit comprising bands of garnet-rich phyllites interbedded with meta-greywackes. The formation of this mineralised schist unit is attributed to the percolation of exhalative fluids, precipitating metal-rich chemical sediments (Flottmann et al., 1996).

3 Kanmantoo Mine area

3.1 Local geology

The Kanmantoo Cu-Au deposit and proximal area(s) are associated with three major rock types: quartz-mica schist, quartz-biotite-garnet-andalusite±chlorite±staurolite rock, and biotite-garnet-chlorite±staurolite schist which hosts much of the sulphide mineralisation (Pollock et al., 2018), and occurs within the garnet-andalusite-biotite schist and garnet-andalusite-biotite-staurolite schist. In addition to this, exhalative rocks were recognised by Toteff (1999) in quartz-mica schist and garnet-andalusite-biotite schist within 3 km of the Kanmantoo Mine manifested as spessartine garnet-quartz rocks, banded iron formation, magnetite-rich andalusite schist and albitite.

3.2 Regional mineralization, metamorphism and veins

The mineralisation at the Kanmantoo Mine and proximal areas is hosted by the Tapanappa Formation and occurs predominantly as chalcopyrite along with variable levels of disseminated pyrrhotite, magnetite, pyrite, covellite, chalcocite and sphalerite (Seccombe et al., 1985; Parker, 1986; Oliver et al., 1998; Schiller, 2000; Abbot, 2005), with debated origin of mineralisation (Oliver et al., 1998; Lyons, 2012; Mauger et al., 2018) whether a consequence of post-Delamerian igneous intrusions during Early Ordovician (483±2.5 Ma; Kimpton, 2018), a pre-metamorphic, syn-sedimentary origin (Seccombe et al., 1985) or a syn-metamorphic genesis (Thomson, 1975).

The eastern Mt. Lofty Ranges is a complex region with numerous thrust faults, shear zones and folds. The Kanmantoo Mine area lies within the regional Kanmantoo Syncline which is a D_2 structure plunging ~15°S. Within the Kanmantoo Syncline, the western limb bears indistinct bedding and shear planes subparallel to the S_2 schistosity while the eastern limb has clearly defined bedding with occasional shear planes (Schiller, 2000; Pollock et al., 2018). The S_2 schistosity (associated with D_2 event) is the best-preserved fabric in the region, generally trending north-south (Spry et al., 1988; Oliver et al., 1998). The D_3 event in the Kanmantoo Mine area is usually observed as gentle crenulations and kinks (Schiller, 2000). The Kanmantoo Mine area lies in the andalusite-sillimanite zone (Fig. 1b), and the metamorphic character can be best described as Buchan-style metamorphism, consisting of high-T, low-P conditions exemplified by the presence of andalusite indicating peak conditions of 550°-600°C and pressures of 3-5 kbar (Offler and Fleming, 1968; Mancktelow, 1990; Dymoke and Sandiford, 1992). At Kanmantoo Mine and proximal areas, numerous episodes of tectonic activity are observed supported by the identified multiple mineral (garnet, staurolite, andalusite) growth events, intrusion of deformed and undeformed felsic and quartz veins (c. 495-483 Ma, Kimpton, 2018), presence of aluminous segregations dated at c. 498 Ma (Kimpton, 2018), and late-stage Cu- and Au-Bi mineralisation in the region. In general, the rocks at Kanmantoo Mine are host to two generation of staurolites and garnets interpreted to have formed in response to extensive metasomatic activities. Locally, during late- to post- peak-metamorphic period, Cu-mineralisation occurred at c. 492-485 Ma, co-eval with post-Delamerian extensional regime at c. 490 Ma (Lyons, 2012).

Numerous igneous intrusions characterised as syn- to post-Delamerian Orogeny (Foden et al., 2006) have been observed within 50 km radial radius of the Kanmantoo Cu-Au deposit. Various deformed and undeformed quartz, felsic and quartz-muscovite veins, rich and devoid of aluminous segregations occur within the region, often concordant and occasionally discordant to bedding. Majority of these veins overprint all pre-existing pervasive features in the host rocks. Gum (1998) observed quartz-muscovite veins 10 km west of the deposit intruding along late shear zones and documented the quartz-muscovite vein-rich Monarto granite. Regionally, variety of late-stage intrusions have been identified.

4 Methodology

4.1 Sample selection, microstructure and microchemistry

Samples were selected to address the problem in question—determining the timing of Delamerian deformation events in units near Kanmantoo Mine, located approximately 2 km south of the town of Kanmantoo, and constrain the timing of depositional/deformation near Long Valley Road by undertaking $^{40}Ar/^{39}Ar$ geochronology.

190   To do this, we sampled a phyllite (sample 2746269) near Long Valley Road representative of the Backstairs Passage Formation unit truncated by quartz-muscovite vein (sample 2746268) (Fig. 2a). In addition to this, we also sampled a two-mica schist (sample 2746272) representing regional schist of the Tapanappa Formation from a zone between two coarse-grained psammitic units (Fig. 2b) displaying well-defined mica foliation which locally develops late-stage crenulations. The unit is host to numerous veins, from which two representative quartz-muscovite veins were sampled- sample 2746270 which is a boudinaged variety and

195   sample 2746271 which is non-boudinaged (undeformed) quartz-muscovite vein. Table 1 presents sample summary for this study.
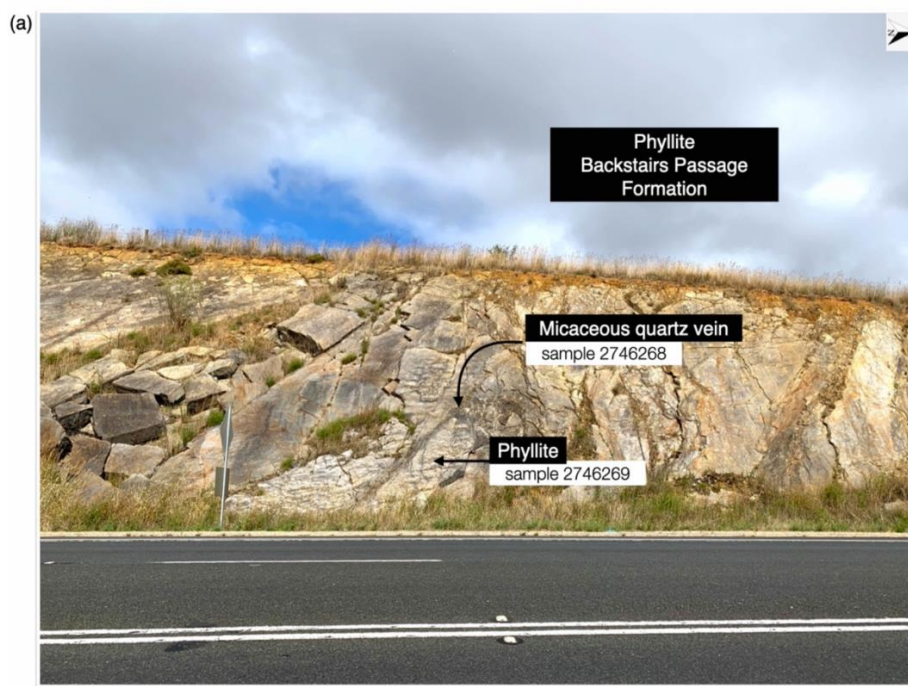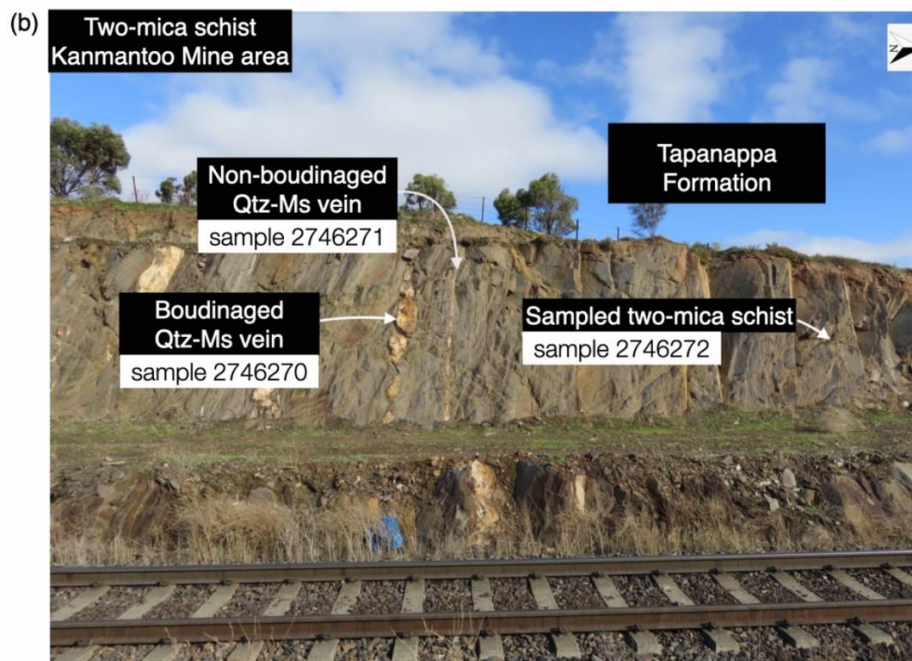
Figure 2. (a) Backstairs Passage Formation of Kanmantoo Group outcropping at Long Valley Road (35°10'36'' S, 138°53'26'' E) and (b) Tapanappa Formation of Kanmantoo Group in cross section view outcropping near Kanmantoo Mine (35°06'04''S, 138°59'56''E).

Sample	Lithology	Stratigraphic unit	Mineral analysed	Location	Latitude	Longitude
2746268	quartz-muscovite vein	Backstairs Passage Formation	white mica	Long Valley Road	35°10'36"S	138°53'26"E
2746269	phyllite	Backstairs Passage Formation	biotite-white mica composite	Long Valley Road	35°10'36"S	138°53'26"E
2746270	boudinaged quartz-muscovite vein	Tapanappa Formation	white mica	Kanmantoo Mine area	35°06'04"S	138°59'56"E
2746271	non- boudinaged quartz-muscovite vein	Tapanappa Formation	white mica	Kanmantoo Mine area	35°06'04"S	138°59'56"E
2746272	two-mica schist	Tapanappa Formation	biotite-white mica composite	Kanmantoo Mine area	35°06'04"S	138°59'56"E

Table 1. Sample details

Microstructure analyses were conducted on two polished thin sections from the host rock formations (sample 2746268 and 2746272) on a LEICA DC 500 microscope at the Research School of Earth Sciences, Australian National University (ANU) followed by microchemistry analyses performed on silicates from sample 2746272 JEOL 8530F Plus Electron Probe Microanalyzer at the Centre for Advanced Microscopy, ANU. All analyses were operated with an accelerating voltage of 15kV, a beam current of 10nA, and a beam diameter of 10μm with a counting time of 30s. A maximum of 3 analyses per grain was performed on each sample. The results are discussed later in the paper.

4.2 Sample preparation and neutron irradiation

The first step in sample preparation is sample selection by physical segregation of structures e.g., biotite forming fabric in the sample or different generations of white mica present. Following sample selection, desired mineral aliquots were prepared by standard crushing and sieving followed by routine magnetic separation methods at varying amperage to obtain clean and pure separates. The final step was to handpick the grains under a binocular microscope to acquire the purest fraction possible (>99% purity). Once packed, the samples were then subjected to neutron irradiation in the core of the reactor with suitable flux monitors to calculate J-factor, and salts (K_2SO_4 and CaF_2) to correct for isotopic interferences. Irradiation of sample

batches was done at UC Davis MNRC nuclear reactor in California employing a biotite standard GA-1550 (K-Ar age of 99.18 ± 0.142 Ma; intercalibration from Spell and McDougall, 2003). The samples presented in this study were analysed in two sample batches, ANU CAN#33 and CAN#35. Complete analytical details are provided in Supplement 1.

225

Following irradiation, once the samples 'cooled' to acceptable radiation levels, they were subjected to $^{40}Ar/^{39}Ar$ geochronology at the Research School of Earth Sciences, ANU, involving temperature-controlled furnace step heating diffusion experiments on individual mineral separates, through an ultrahigh-vacuum extraction line connected to a *Thermo Fisher* ARGUS-VI multi-collector mass spectrometer.

230

Prior to measurement, each mineral aliquot id dropped into a temperature-controlled resistance-furnace, and then warmed for a minimum period of 12 hours at c. 350-400°C under ultra-high-vacuum (UHV) conditions to clean the aliquot of deeply penetrated volatiles in fast-diffusion pathways. Flux monitors were analysed employing laser fusion technique using a CO_2 continuous wave laser and step-heating

235 experiments were carried out in temperature-controlled furnace ranging from 450°C to 1450°C involving 30 steps to allow revelation of high-resolution age gradients. After each heating step, gas is released into the mass spectrometer and 51 simultaneous measurements made of the counts (on each Faraday cup) for isotopes ^{36}Ar, ^{37}Ar, ^{38}Ar, ^{39}Ar, ^{40}Ar for approximately 10 minutes. These are then used in a complex data calculation using *Noble 2020* software which in essence removed the effect of isotopic interferences,

240 system background, mass discrimination and atmospheric contamination and then allowed the calculation of age. ^{40}K abundances and decay constants used were calculated as in Renne et al. (2011). Detailed results for each step-heating experiment are presented in Supplement 2, with summary of these ages presented in Table 3. Weighted mean ages are calculated using three or more steps based on Pearson's chi statistics within 95% confidence limit and calculated using the in-house developed software eArgon (see

245 Muston et al., 2021) for detailed description of the statistical method employed.

A proper step-heating schedule is vital for extracting maximum information from the mineral. Loss of crucial data can occur if carefully planned schedules are not employed for e.g., an experiment starting at a high temperature could result in obscuring useful data due to mixing of gas from domains of variable retentivity

250 (thus variable ages) or employing few steps could conceal age gradients that may otherwise emerge in an experiment with generous number of steps.

5 Results
5.1 Field observations
255 The Backstairs Passage Formation unit of the Kanmantoo Group is dominated by massive exposures of foliated phyllite trending roughly N-S. Here, the micaceous unit is underlain by coarse quartzite (bedding S_b; 336/50E; strike/dip) (Fig. 3) host to abundant quartz-mica veins, joints and intense weathering. Two sets of cross cutting fabrics are observed- a primary foliation fabric (S_p) truncated by younger crenulation fabric (S_{cren}) are observed in the phyllitic unit (Fig. 3b). Reverse younging (graded bedding) is observed in

260 the underlying quartzite unit.

Backstairs Passage Formation
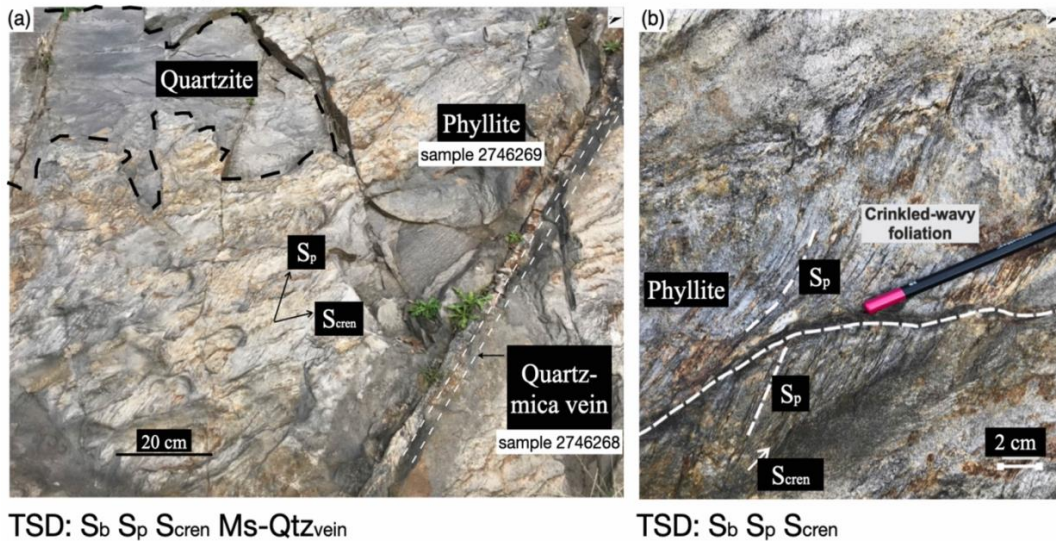
Figure 3. Field exposures of the Backstairs Passage Formation unit at Long Valley Road with tectonic sequence diagrams at the
bottom. (a) host phyllite underlain by quartzite and truncated by quartz-muscovite vein. (b) two sets of fabrics observed in the phyllite.
(S_b: bedding, S_p: primary foliation fabric, S_{cren}: secondary crenulation fabric).

The Tapanappa Formation has extensive exposures near the Kanmantoo Mine. The dominant lithology is
strongly foliated, rheologically less competent two-mica schist roughly trending N-S, packed between
quartz-rich psammitic units (Fig. 4). Here, the primary fabric (S_p) (174/76E; strike/dip) defined by biotite-
white mica schistosity is parallel to the bedding (S_b) (026/66E). At most places, schistosity is concordant
with bedding, however this is not a consistent feature of the outcrop.

Tapanappa Formation

265

270
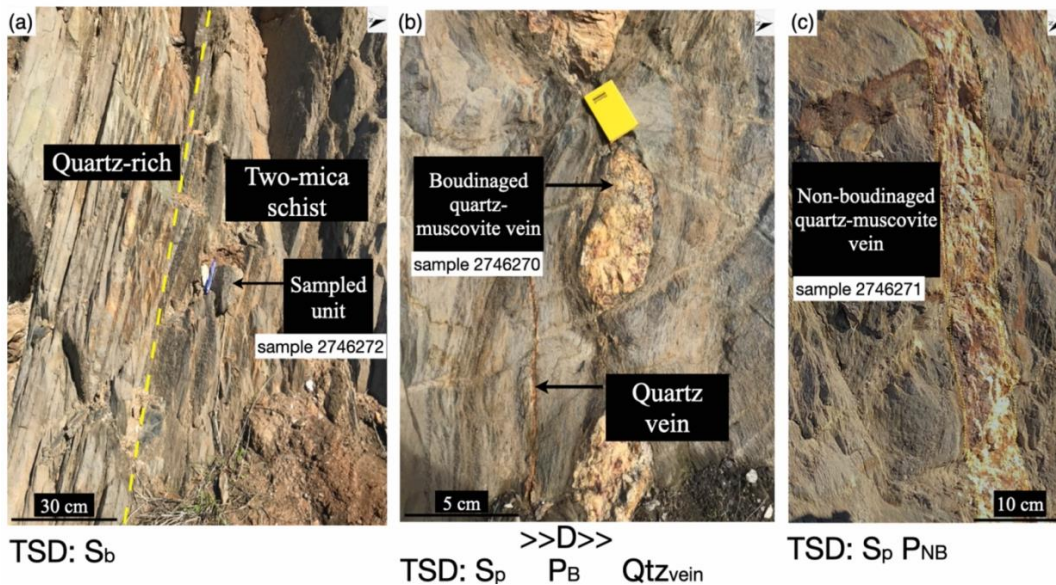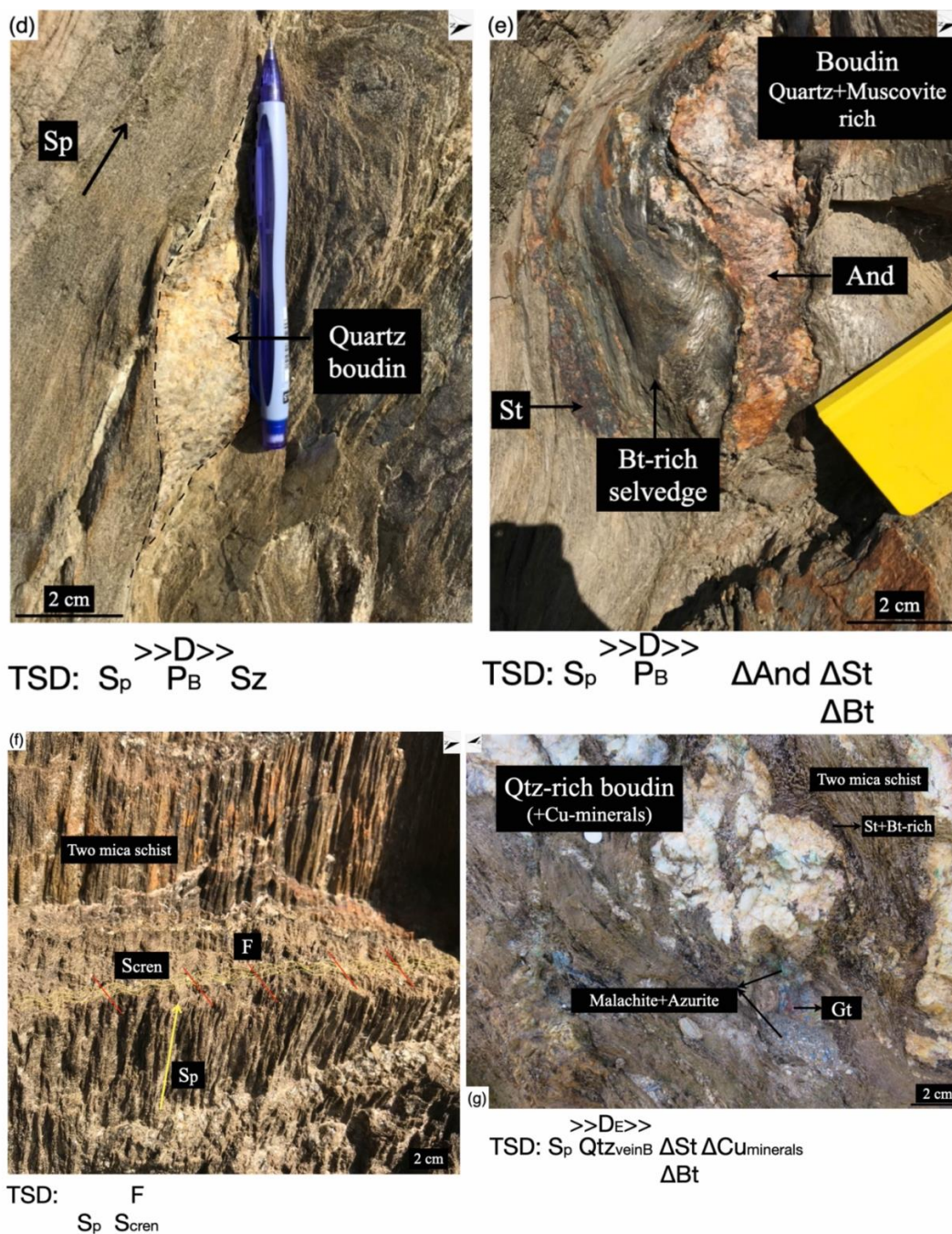
275

280

Figure 4. Field exposures of the two-mica schist at Kanmantoo Mine area with their respective tectonic sequence(s) written at the bottom of each image. (a) two-mica schist, (b) boudinaged quartz-muscovite vein intruding the schist, (c) non-boudinaged quartz-muscovite vein. (S_b: bedding, P_B: boudinaged vein, D: unknown deformation event, S_p: primary fabric, P_s: non-boudinaged vein), (d) quartz boudin, (e) quartz-mica boudin with a biotite-staurolite rich selvedge, (f) late stage S_cren fabric associated with a folding event and (g) malachite and azurite in quartz boudins.

The unit has schistosity layer parallel quartz vein(s) and quartz-muscovite vein(s), which at some places are orthogonal to the fabric. Unmineralized to mineralised and deformed (boudinaged) to undeformed veins occur throughout the unit (Fig. 4d). The massive, boudinaged quartz-muscovite veins occasionally contain pink andalusite and rare garnet. The melt selvedge at the host-quartz-muscovite vein contact is biotite-rich with rare staurolite occurrences (Fig. 4e); however, this is not observed for pure quartz veins. Several boudinaged, schistosity parallel quartz veins are associated with Cu-mineral phase(s). Later stage crenulations, S_{cren}, possibly associated with a younger deformation event, are observed occasionally (Fig. 4f), gently folding the early schistosity along with late-stage faults displacing the quartz-muscovite veins. The unit shows patchy Cu-mineralisation with disseminated azurite and malachite precipitates (Fig. 4g). Locally, irregular occurrences of ptygmatic, unmineralized quartz veins discordant to schistosity are indicative of crumpling of an original planar vein by subsequent compression of the incompetent host.

5.2 Microstructure analyses
5.2.1 Importance of microstructures

Microstructural analyses help in studying the textural relationships in a sample, determination of deformation/thermal events indicated through the presence of index minerals and in understanding the intragrain character of the minerals present. High power transmitted light microscopy was undertaken on thin sections to study the minerals presents, deformation characteristics and recrystallisation (if any), preservation of relict minerals and relative grain sizes present. This is a key step in $^{40}Ar/^{39}Ar$ geochronology because the modification(s) in original microstructures and newly produced microstructures is correlated to the variation(s) in ages reflected in the age spectrum of the mineral, where different ages can often be correlated with different event(s) and/or element(s) of a microstructure.

In routine, age determination and interpretation are preceded by careful examination of the target mineral (in this case biotite, white mica and mica composites) by optical microscopy and microchemical analyses. Following this, microprobe analyses were conducted on thin section for phase characterisation and determination of chemical character for minerals described in detail in section 5.4. Results for microchemical analyses are presented for sample 2746272 (two-mica schist, Tapanappa Formation) only. Sample 2746269 (phyllite, Backstairs Passage Formation) was not subjected to microchemical analyses due to its very fine-grained texture.

5.2.2 Backstairs Passage Formation, Long Valley Road

The sample is a phyllite with interlayered biotite-white mica grains. At the outcrop scale, two sets of cross-cutting fabrics were observed (Fig. 3), which are also visible at the microscopic scale (Fig. 5). The younger fabric, biotite-mica rich crenulation cleavage domain (S_{cren}) is regularly spaced, parallel and anastomosing. S_{cren} sharply truncates the older differentiated cleavage fabric (S_{diff}) and is nearly orthogonal to it. This younger fabric is not penetrative and is observed only in the top half of thin section (Fig. 5a) corresponding to the top layer of the sampled unit. Within this sample area, S_{diff} is observed to merge and transition smoothly into S_{cren} occasionally, where the sample is dominantly mica-rich and quartz-poor. In the microlithons, the S_{diff} fabric is defined by interlayered biotite+white mica that display gentle to strong kinking, and occasional strong bending (microfolds) of the mica-flakes. The microlithons contain interstitial quartz with foam texture (Fig. 5b) indicative of a later heating event resulting in post-crenulation crystallization. Overall, the crenulation cleavage generates microfolds in the older planar fabric and is suggestive of polyphase deformation in this sample.
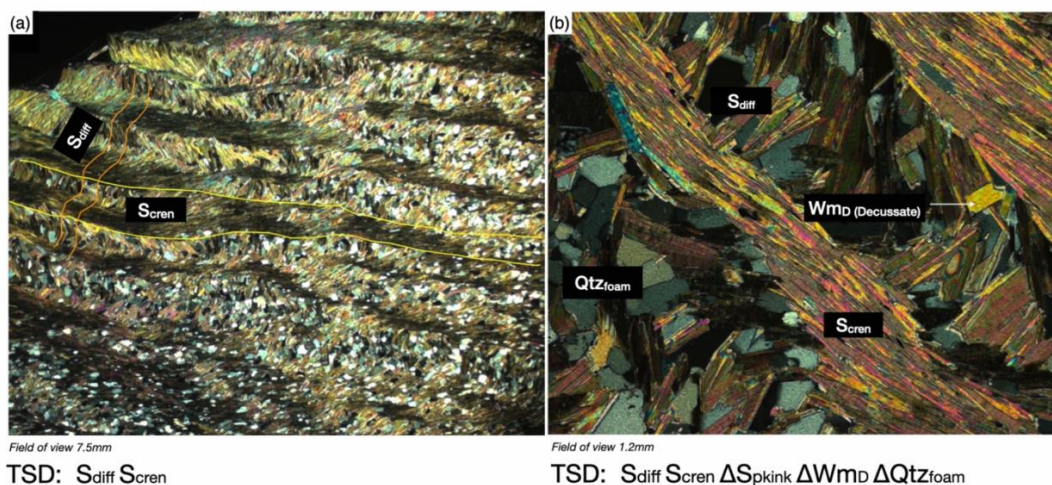
Figure 5. Microstructure observations of phyllite, Backstairs Passage Formation. (a) two sets of fabrics in the phyllite and (b) quartz foam texture in the microlithons and late-stage decussate white-mica. (S_{diff}: differentiated cleavage, S_{cren}: crenulation cleavage, ΔS_{pkink}: kinking of primary fabric S_{diff}, ΔWm_D: growth of decussate white mica, ΔQtz_{foam}: formation of quartz foam texture).

5.2.3 Tapanappa Formation, Kanmantoo Mine area

The two-mica schist consists of interlayered biotite+white mica, quartz, garnets, chlorite, rare relict poikiloblastic staurolites and sulfides. The staurolites grow over a relict, older fabric demonstrated by white mica inclusion trails (termed as first generation, Wm_1; the subscript denotes generation sequence). The sample displays a prominent schistosity (S_p) defined by fine-grained intercalated biotite+white mica (Bt_1+Wm_2), some altering to chlorite (Chl_{Sp}) (Fig. 6h), occasionally displaying a decussate texture. Chlorite (Chl_{Sp}) is observed overgrowing this foliation at places, possibly at the expenses of micas, and is likely distinct to the chlorite growing in the staurolite pressure-shadow (Chl_{St}) (Fig. 6c).

The schistosity (younger) wraps around relict staurolite pods, breaking down to white mica, foam textured quartz, minor chlorite (Chl_{St}) and scarce, heavily fractured andalusite grains with sericite along fractures, likely to have formed co-eval with, and in response to the deformation forming S_p fabric and destabilising staurolites (Fig. 6b). The white mica (Wm_3) forms a coarse rim around relict staurolite grains, thus preventing their further consumption (Fig. 6a). The S_p fabric bears a different orientation relative to the inclusion trails in the staurolites. The white micas in the staurolite pressure-shadows are coarser and are not aligned to the external S_p fabric (Fig. 6a). Cross cutting this third generation of white micas are the decussate ones (Wm_D) (Fig. 6a), interpreted as last in the sequence of white mica formation. Small, euhedral to subhedral garnets overgrow the primary schistosity absent any obvious deformation features, and are interpreted to have formed during the last stages of deformation history (Fig. 6d-f). The schist bears two types of garnets, fractured and altered (Gt_{Al}), non-fractured and unaltered (Gt), suggestive of two episodes of garnet growth. Back scattered electron imaging (BSE) of the fractured garnets shows precipitation of secondary biotite±chlorite±polygonal quartz mostly in and around fractures, and occasionally biotite±chlorite rimming the garnet core (Fig. 6d-g).

TSD: ΔWm₁ ΔSt Sp (Bt₁+Wm₂) ΔWm₃ ΔWm_D ΔGt_Al ΔGt ΔQtz_foam

360

TSD: Sp (Bt₁+Wm₂) ΔAnd ΔGt_Al ΔQtz_foam
ΔWm₃

TSD: Sp(Bt₁+Wm₂) ΔWm3 ΔQtz_foam
ΔChl_St
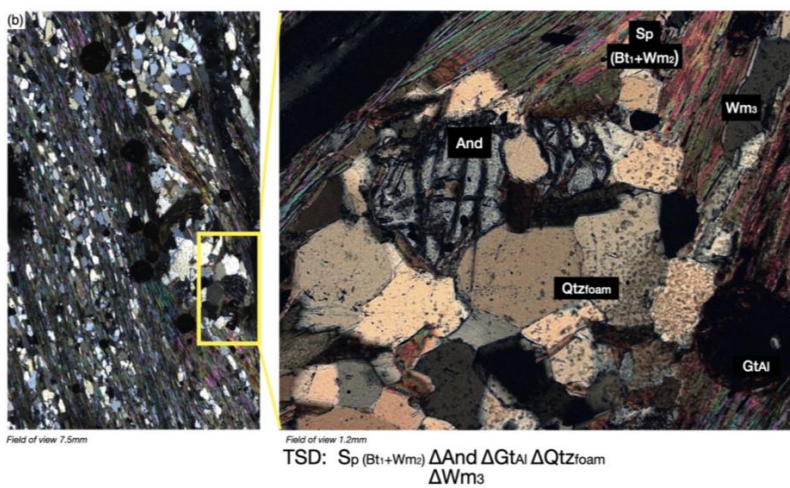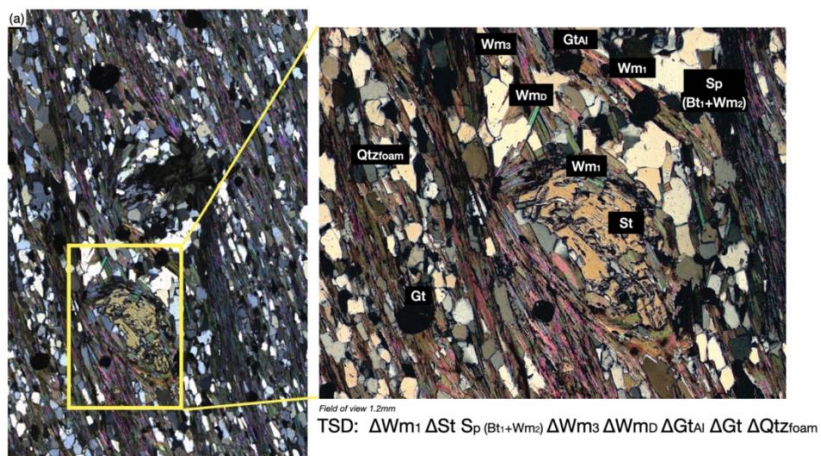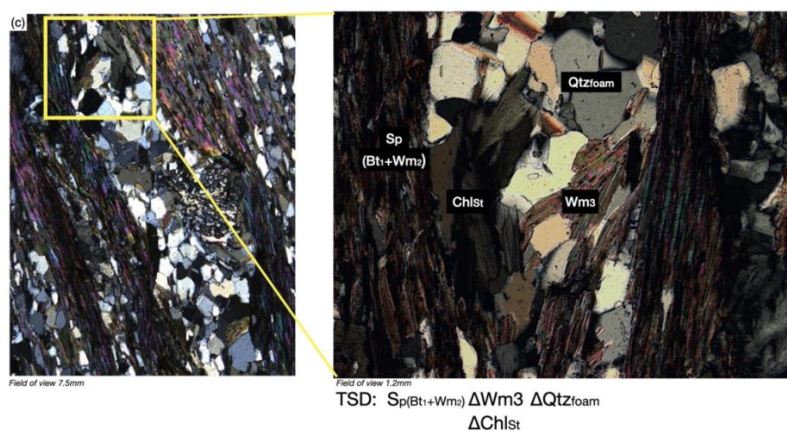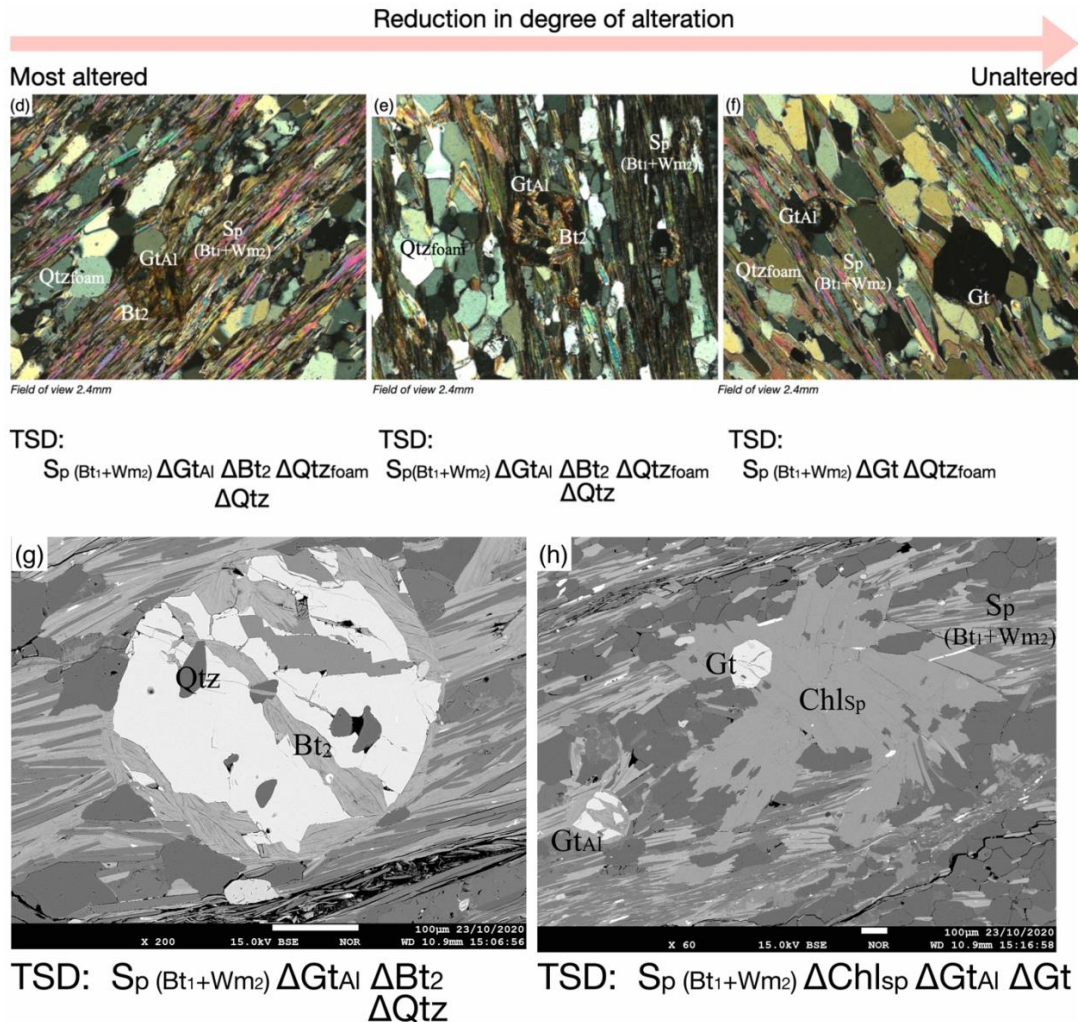
Figure 6. Microstructure observations of biotite schist, Kanmantoo Mine area. (a) relict staurolites overgrowing older fabric defined by white mica inclusion trails, (b) and (c) sericite altered andalusite and chlorite growing in staurolite pressure shadows, respectively. (d), (e) and (f) show degree of alteration in garnets with most altered garnets proximal to schistosity. (g) and (h) late-stage static garnets overgrowing the schistosity. (S_p: primary fabric (schistosity), Wm_n: white mica of generation 'n', Bt_n: biotite of generation 'n', Chl_{Sp}: chlorite overgrowing S_p, Chl_{St}: chlorite growing in staurolite pressure shadow, Gt: garnet, Gt_{Al}: altered garnet)

5.3 Tectonic Sequence Diagrams (TSDs)

Here, we have adopted the method of Tectonic Sequence Diagrams or TSDs proposed by Forster and Lister (2008), that allows the systematic recording of all deformation and metamorphic events (e.g., mineral growth events), subsequent overprinting events (if any) and estimating their duration. Tectonic sequence diagrams allow easy representation of maximum information from one key location/outcrop, that can be correlated to features on regional scale with an added advantage of adding any information later obtained. Thus, later recorded events (if any) can be easily added to or omitted from any part of the tectonic sequence diagram using annotations as outlined in Table 2.

Annotation	Description
S_b	Bedding

S_p	Primary fabric (foliation/schistosity)
S_{cren}	Secondary fabric (crenulation cleavage)
P_B	First quartz-muscovite vein (boudinaged) event
P_{NB}	Second quartz-muscovite vein (non-boudinaged) event
Qtz_{vein}	Undeformed quartz-vein
Qtz_{veinB}	Boudinaged quartz vein
D	Unspecified deformation event
F	Folding related to unspecified deformation event
ΔBt_1	Growth of first-generation biotite
ΔBt_2	Growth of second-generation biotite
ΔGt_1	Growth of first-generation garnet
ΔGt_2	Growth of second-generation garnet
ΔAnd	Andalusite mineral growth event
ΔSt	Staurolite mineral growth event
$Qtz\text{-}Ms_{vein}$	Quartz-muscovite vein
ΔQtz_{foam}	Quartz (foam-texture)
ΔChl_{Sp}	Chlorite overgrowing S_p fabric
ΔChl_{St}	Chlorite growing in staurolite pressure shadow
ΔWm_D	Decussate white-mica growth event
$>>_D>>$	Duration of specific event e.g., deformation
$\begin{array}{c} S_2 \\ \Delta Bt1 \end{array}$	Two events in a sequence occurring synchronously, one below the other; biotite growth during S_2 fabric

Table 2. Annotation used in tectonic sequence diagram for structural features and mineral growth events

Delamerian Orogenesis is a complex event, the nature and lifespan of which has not been fully worked out. The exposures observed at both locations are puzzling and, therefore their structural analyses are imperative. Therefore, there was a need for considering older numerical schemes as secondary and new methods of recording sequences to be adapted.

Here, we have produced a simplified tectonic sequence diagram for both units, the phyllite of Backstairs Passage Formation, and the two-mica schist of Tapanappa Formation, where multiple event sequences inferred through generations of fabrics and intrusions observed at key points have been determined in a single outcrop. Thin section analyses provide constraints on the relative timing of events, and information on structures that are not observed at hand-specimen scale. Therefore, the presented final sequence also includes microstructural input observed during detailed petrographic analyses.

The TSD inferred from observations as outcrop scale of the phyllite of Backstairs Passage Formation matches well with that observed as microstructure scale. From Fig. 3 the sequence is defined as:

$$S_b \; S_p \; S_{cren} \; Qtz\text{-}Ms_{vein}$$

At microstructure scale (Fig. 5), the sequence is defined as:

$$S_p \; S_{cren} \; \Delta S_{pkink} \; \Delta Wm_D \; \Delta Qtz_{foam}$$

The final tectonic sequence thus becomes:

405 S_b S_p S_{cren} ΔS_{pkink} *ΔWm_D ΔQtz_{foam} $Qtz\text{-}Ms_{vein}$*

The Tapanappa Formation at the Kanmantoo Mine area has an intense bedding parallel foliation fabric (S_p), which locally diverges from bedding (S_b). S_p has layer parallel quartz-muscovite veins (deformed and undeformed) with secondary mineral(s) precipitating at vein-host contact. From Fig. 4 the inferred compiled
410 sequence at outcrop scale is defined as:

$$>>>D>>>$$
S_b S_p *F* Qtz_{veinB} P_B $\Delta And\Delta St$ S_z P_{NB} Qtz_{vein} $\Delta Cu_{minerals}$
      S_{cren} ΔBt

415

At microstructural scale (Fig. 6), more complex relationships are observed. The observed sequence is defined as:

ΔWm_1 ΔSt S_p ΔWm_3 ΔWm_D ΔChl_{Sp} *ΔGt_{Al}*   *ΔGt* ΔBt_2 ΔQtz_{foam}
420   ΔAnd ΔQtz
        ΔChl_{St}

Integrating field and microstructural observations, the final sequence becomes:

425 $$>>D>>$$
S_b ΔWm_1 ΔSt S_p ΔWm_3 ΔWm_D *ΔChl_{Sp}* *F* Qtz_{veinB} P_B ΔAnd ΔSt ΔGt_{Al} ΔGt ΔBt_2 ΔQtz_{foam} *P_{NB}* Qtz_{vein} $\Delta Cu_{minerals}$
     ΔAnd   *S_{cren}*   *ΔBt*   *ΔQtz*
     ΔChl_{St}

430 *Note: The parts of segments in italics signify the uncertainty in the sequence of event(s).*

5.4 Mineral compositions

Electron-microprobe analyses of silicates (garnet, biotite, muscovite, chlorite and quartz) were obtained from the Tapanappa Schist of the Kanmantoo Mine area. Complete details of analytical setup are provided
435 in Supplement 3 and representative major and minor elements for the mineral phases of the Tapanappa Schist are provided in Supplement 4 in the electronic supplement. In summary, the garnets in the sample show a narrow range of MgO wt.% compositions (2.36-2.43 wt.%), are rich in total FeO ranging between ~29-31 wt.% and MnO compositions between ~7-8 wt.%. The biotite mica in the sample shows a compositional range with values of 9-10 wt.% MgO and 17-18 wt.% FeO along with consistent minor
440 concentration of TiO_2 of ~1.5 wt.%.

5.5 $^{40}Ar/^{39}Ar$ age spectra results

Age spectrum analyses were undertaken using e*Argon* multifunctional software designed in-house at the Research School of Earth Sciences, Australian National University, that allows data representation using
445 different plot types. Here, data has been analysed using the age-spectrum plot and Arrhenius plot, where the age-spectrum represents apparent ages (Ma) in a mineral as a function of ^{39}Ar release with temperature increments in steps and therefore, makes it possible to identify different age populations. The Arrhenius plot analyses was undertaken in conjunction with the age spectrum analyses and allows for identification of distinct age domain(s) within a mineral and estimation of their activation energies (E_a) and closure
450 temperatures (T_c). This was achieved by employing The Fundamental Asymmetry Principle (FAP) of Forster and Lister (2010) in which steps in a heating experiment are divided by rank order and slope of the line corresponds to an activation energy value. This approach allows for estimation of diffusion parameters for the age domain in question with values less than or equal to the actual value.

455 **5.5.1 Backstairs Passage Formation, Long Valley Road**

Sample 2746269 is a phyllite from the Backstairs Passage Formation unit composed of biotite-white mica composite grains, and abundant quartz with two sets of deformation fabrics. Biotite-white mica composites from this sample present a simple age spectrum rising asymptotically from a minimum age of c. 388 Ma to

460 an upper limit age of 484±1.1 Ma at ~20% ^{39}Ar release (Fig. 7a). The spectrum shows a subtle dip around 60% gas release with a minimum age of 481±1.5 Ma. Following this, there is a gradual increase in apparent age reaching a maximum of c. 506 Ma in the high temperature steps of the experiment. In summary, ages range from c. 484-481 Ma with ^{39}Ar gas release from ~10-95%. A correlation is observed between the Ca/K ratio plot and age spectrum where a spike in Ca/K ratios (degassing of fluid inclusion/contaminant etc that may contribute ^{40}Ar$_E$) at c. 30% ^{39}Ar release is observed (Fig. A2, Supplement 1), that contributes to the

465 sub-plateau age of c. 484 Ma identified in the age spectrum.
The biotite-white mica grains in the thin section show intimate growth in the two sets of deformation fabrics, S_{diff} and S_{cren}. The modal abundance of decussate white mica in the sample is relatively low, and thus it would be safer to assume no to minimal contribution from this white mica to the age spectrum. The age variation evident in the age spectrum could be due to mica composite contributions from the two sets of

470 deformation fabrics. However, the relatively smaller age variation observed in the age spectrum is suggestive of continuous biotite-white mica growth during fabric formation. Therefore, the ages obtained in the age spectrum display variations preserved in the individual minerals forming the composite crystals that could degas preferentially during step-heating experiments, and therefore, we cannot disregard the complexity introduced through the composite nature of the mineral separate used.

475

Sample 2746268 is a micaceous quartz vein (Fig. 7b). The age spectrum for white mica from this sample rises from a minimum age of c. 318 Ma, reaching an upper limit age of 476±2.3 Ma, followed by a dip in apparent ages at 50% ^{39}Ar release, where a minimum semi-plateau age of 468±1.4 Ma is observed. Towards the high-temperature steps of the experiment, the age spectrum displays unusually older apparent

480 ages at ~95% ^{39}Ar release, and thus, these steps are not employed for age assessment purposes. This could be due to abrupt degassing of any trapped contaminants or material that is not rich in radiogenic argon as the radiogenic argon content decreases from 80% to 20% rapidly (Fig. A1, Supplement 1). The closure temperature value estimates of 313°-329°C are obtained for this sample using Arrhenius plot analyses (Supplement 1). The Ca/K ratio plot shows degassing of a potential Ca-rich component (fluid

485 inclusion/contaminant decrepitation that may contribute ^{40}Ar$_E$.) at c. 54% ^{39}Ar release with a Ca/K ratio of c. 1.5, corresponding effects of which are observed in the age spectrum and %^{40}Ar* radiogenic plot with very similar overall pattern in the two plots (Supplement 1).
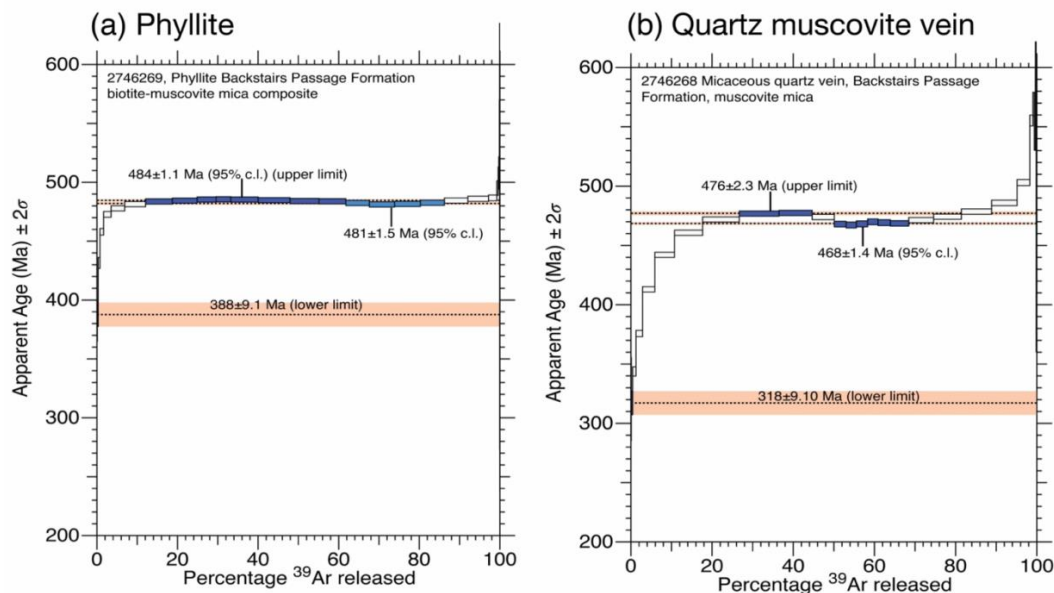
Figure 7. Age spectra from (a) biotite-white composite from phyllite and (b) white mica from quartz-muscovite vein of Backstairs Passage Formation

5.5.2 Tapanappa Formation, Kanmantoo Mine area

Sample 2746272 (Fig. 8a) is a two-mica schist displaying a disturbed age spectrum. Biotite-white mica composite grains from this sample display an age spectrum stepping upwards from a minimum age of c. 203 Ma. A mica sub-spectrum is observed in the first 20% of ^{39}Ar release with two steps defining an age of 496±1.7 Ma. Following this, a subtle decline in apparent ages at ~20% ^{39}Ar release with an age of 488±1.6 Ma. The spectrum then rises gradually, reaching an upper limit age of 506±2.3 Ma at ~60% ^{39}Ar release. Following this, a gradual fall in apparent ages is observed, with two steps at ~84% ^{39}Ar gas release defining an age of 498±1.6 Ma. The higher temperature steps of the experiment are avoided for age interpretation due to very low radiogenic argon content (~60%) (Fig. A5, Supplement 1). There exists a good correlation between age spectrum and Ca/K ratio plot (Supplement 1). No obvious correlation is observed with Cl/K ratio plot.

Sample 2746270 is a boudinaged quartz-muscovite vein truncating the host two-mica schist. White-mica dated from this quartz-muscovite vein delivers a simple age spectrum with an older apparent age of 531±3.6 Ma defined by two steps as observed in the muscovite sub-spectrum in the first 4% of ^{39}Ar release (Fig. 8b). The spectrum then shows a rapid decrease in apparent ages, reaching a semi-plateau age of 492±1.7 Ma comprising of 3 steps with nearly 50% of ^{39}Ar release. Towards the higher temperature end of the experiment, a second semi-plateau comprising ~30% ^{39}Ar release with an age of 495±1.1 Ma is observed. The terminal heating steps in the experiment (>95% ^{39}Ar release) are not used in the age analyses due to their low radiogenic argon release contribution (60%-40%) (Fig. A3, Supplement 1). A closure temperature range of 297°-535°C has been estimated employing Arrhenius plot analyses (Supplement 1). Effects of ^{39}Ar recoil are observed in the initial heating steps of the experiment. No obvious correlation is observed with Cl/K ratio plot (Supplement 1).

Sample 2746271 is a white-mica separate from non-boudinaged quartz-muscovite vein and has a similar degassing pattern to the boudinaged quartz-muscovite vein (Fig. 8c). The sample preserves an older age of 519±6.5 Ma observed in the muscovite sub-spectrum in the first 4% of ^{39}Ar release. The age spectrum remains relatively flat for most part of the experiment and shows a uniform plateau age of 493±0.9 Ma comprising approximately 70% ^{39}Ar release. No obvious correlation is observed with Cl/K ratio plot (Fig. A4, Supplement 1).

Arrhenius plot analyses (Supplement 1) demonstrates the presence of multiple age domains within the samples at Kanmantoo Mine area. In the host schist, the c. 506 Ma age domain corresponds to an activation energy of 47 kcal/mol. The c. 492 Ma and c. 495 Ma age domain in the mica from boudinaged vein correspond to activation energies of c. 53 kcal/mol and 154 kcal/mol, respectively. The c. 493 Ma age domain from the non-boudinaged vein has contributions from multiple domains of varied retentivity as per the Arrhenius plot with activation energies varying from 52 kcal/mol to 91kcal/mol, however, a single plateau age is observed in the age spectrum and does not reflect any age variation corresponding to changing activation energies. Effects of ^{39}Ar recoil are observed in the initial heating steps of the experiment in this sample.
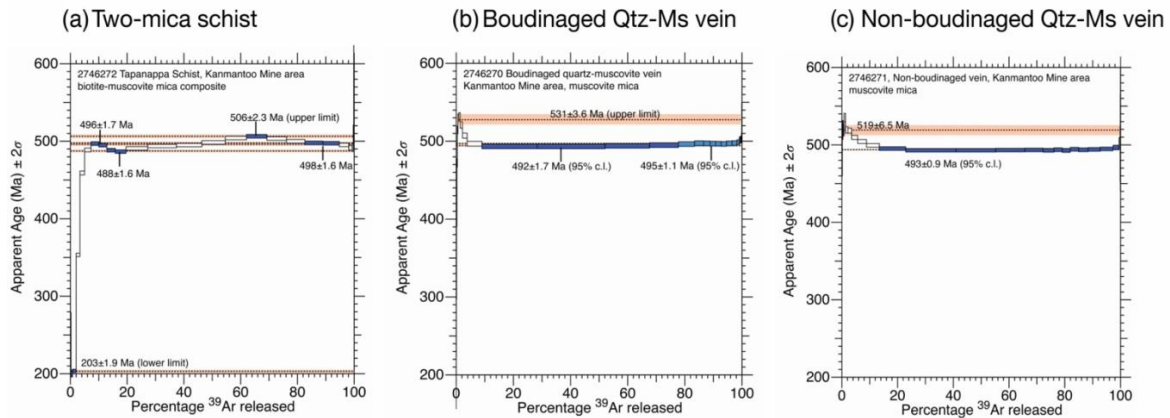
Figure 8. Age spectra of (a) host biotite-schist, (b) Boudinaged quartz-muscovite vein and (c) non-boudinaged quartz-muscovite vein.

The Arrhenius plot for the host phyllite and biotite schist in this study is presented in Fig. 9. Both samples have distinct age domains with varied retentivities expressed in terms of their activation energies and closure temperatures estimated for a moderate cooling rate of 20°C/Ma. Assuming a simplified spherical geometry for the minerals, Arrhenius plot analyses (Fig. 9) estimated closure temperatures of 370°-339°C for the phyllite, and 279°-352°C for the two-mica schist. Table 3 summarizes geochronology data obtained in this study.
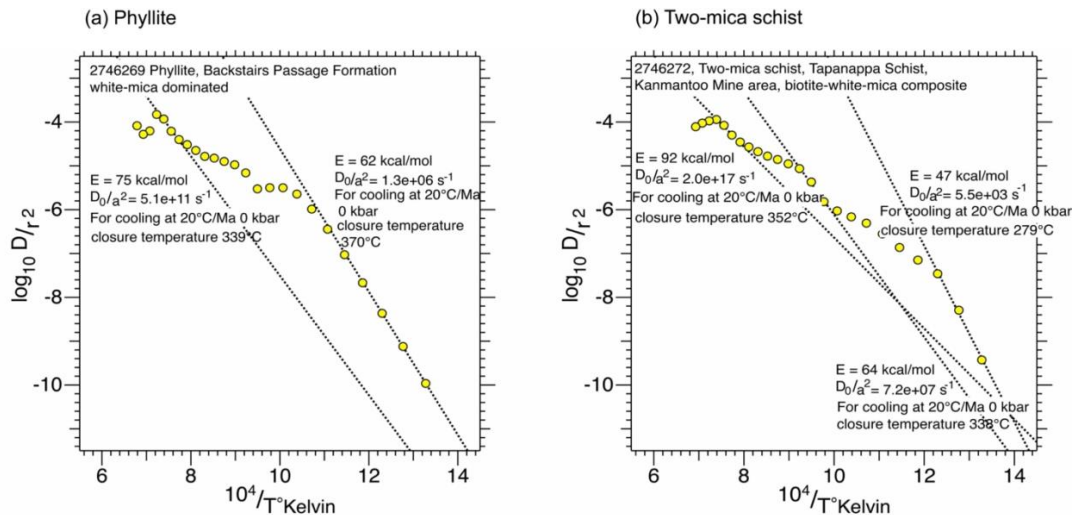
Figure 9. Arrhenius plots for (a) phyllite from Backstairs Passage Formation unit, and (b) two-mica schist from Tapanappa Formation. The plot employs FAP principle of Forster and Lister (2010) to estimate activation energies (E) and closure temperature(s) (T_c).

Sample	Lithology	Stratigraphic unit	Mineral analysed	Interpreted age(s) (Ma) +2σ error	Age type	Interpretation	Estimated closure temperature window (Tc)
2746268	Micaceous quartz vein	Backstairs Passage Formation	white mica	476±2.3	sub-plateau	max. intrusion age	313-329°C

				468±1.4	sub-plateau	min. intrusion age	
2746269	Phyllite	Backstairs Passage Formation	biotite-white mica composite	484±1.1	sub-plateau	max. age of S_{cren} formation or min. age of S_{diff} formation	339-370°C
				481±1.5	sub-plateau	min. age of S_{cren} formation	
2746270	Boudinaged quartz-muscovite vein	Tapanappa Formation	white mica	531±3.6	upper limit	Relict older/inherited age	297-535°C
				495±1.1	sub-plateau	min. formation age of boudinaged vein	
				492±1.7	sub-plateau	effect of younger undeformed vein	
2746271	Non-boudinaged quartz-muscovite vein	Tapanappa Formation	white mica	519±6.5	upper limit	Relict older/inherited age	283-455°C
				493±0.9	plateau age	Min. formation age of non-boudinaged vein	
2746272	Two-mica schist	Tapanappa Formation	biotite-white mica composite	506±2.3	upper limit	Older age component	279-352°C
				498±1.6	intermediate ages	Ages similar to intrusives in the region. Reflects intrusion of boudinaged quartz-muscovite vein	
				496±1.7			
				488±1.6	intermediate limit	max. age of retrogression and garnet growth (inferred)	

Table 3. Summary of geochronology results from this study

550 **6 Discussion**

6.1 What have we dated? Cooling ages vs. deformation/growth ages
One of the key arguments presented while interpreting argon data is deciding whether the ages are cooling ages or if they represent important geological events experienced by the unit in question. Often, this is
555 debated and sometimes it is difficult to present a simple answer.

The Ar-systematics in a mineral are affected by various parameters including and not limited to pressure, ambient temperature, closure temperatures, rate of cooling and composition of a mineral. In general, age spectra with more than one plateau age are often considered 'mineral mixtures', and are interpreted to have
560 preserved information on the timing of different geological episodes of cooling and/or deformation, sometimes referred to as 'rim' and 'core' domains in a mineral preserving varied ages for simple understanding. The rims are usually considered as zones of partial argon loss mantling a core that is essentially closed and/or is more retentive of argon. When a mineral cools, the retentivity begins to increase and the age thus recorded by the mineral depends on its cooling rate and mineral composition among many
565 factors. Ar-closure during rapid cooling occurs at a higher temperature than that for slow cooling and thus, the age preserved is likely to be in close agreement with the true age of the event dated (Lister and Baldwin, 1996). Similarly, a sample held at a higher ambient temperature for geologically significant periods of time would most likely preserve age(s) that may not have any geological significance due to loss of Ar by diffusion. This is sometimes true for plateaus, where well-defined plateaus are considered a characteristic
570 of fast cooling whereas low apparent ages in the initial part of the age spectrum are characteristic of slow

cooling and a staircase morphology represents diffusive Ar-loss. The age spectrum profiles then generated would reflect the nature of cooling and would record different T-t histories (Lister and Baldwin, 1996). The more pronounced staircase nature of the spectrum in the initial parts of the experiment are indicative of slower cooling leading to more diffusive loss of argon and thus preservation of ages which are fair to be interpreted as 'cooling ages'.

To illustrate this concept better, the two locations from this study are explained here where $^{40}Ar/^{39}Ar$ apparent cooling and/or growth/deformation ages can be differentiated. As an example, the age spectra from the Backstairs Passage Formation (Fig. 7) displays a staircase morphology in the initial 20% of ^{39}Ar release for the host phyllite and the quartz-muscovite vein. Following the formation of fabric (S_{cren} and S_{diff}) in the host phyllite between c. 484-481 Ma, the cross-cutting quartz muscovite vein formed between c. 476-468 Ma after the host phyllite had substantially cooled. The age data for the muscovite from quartz muscovite vein shows the growth of a more-retentive white mica domain at c. 468 Ma (Fig. 7b) as it degasses in the higher temperature part of the experiment subsequent to the degassing of c. 476 Ma domain. Similarly, the c. 481 Ma age domain in the host phyllite is interpreted here as a mica growth/resetting event which is linked to the formation of the younger S_{cren} fabric overprinting the older S_{diff} fabric (Fig. 7a). In summary, the younger age components degassing in the high temperature parts of the heating experiment for the host phyllite and the quartz-muscovite vein are understood here as mineral growth/fabric formation ages and not 'cooling ages'. Moreover, the younger age limits in the samples are identified as minimum age constraints on the deformation and/or intrusion in the region, while the older age components constrain the maximum ages of these geological episodes. Furthermore, no geologically meaningful ages could be identified in the initial the 20% of ^{39}Ar release from both age spectra due to diffusive ^{40}Ar loss.

The age spectra for mineral separates from the Kanmantoo Mine area do not display a staircase morphology (Fig. 8) and have well-defined plateaus for sample 2746270 and 2746271. Thus, we interpret these to have cooled rapidly and preserving age(s) closer to or no younger than the true age(s) of the events dated. A sub-spectrum is observed in the first 5% of ^{39}Ar gas release which could be a relict older component. The age spectrum for sample 2746272 (Fig. 8a) shows a steep rise in the initial 10% of ^{39}Ar release, however, no interpretation has been made from this part of the age spectrum.

Thus, the interpreted ages for all units in this study are interpreted in context of the timing or duration of geological episodes at particular locations as outlined in Table 4.2 unless specifically outlined as cooling ages.

6.2 Timing of Delamerian Orogeny at Kanmantoo Mine area - data interpretation and implications

The new $^{40}Ar/^{39}Ar$ data from the Kanmantoo Mine area provide constraints on the timing of deformation in this region. However, we recognise that the Delamerian Orogen experienced a complex deformation and metamorphic history and, inferences drawn from this study, on a limited number of samples must necessarily serve as a foundation for further studies and are not intended to define the timing and duration of the Delamerian Orogeny as a whole.

The two-mica schist in the Kanmantoo Mine area, sample 2746272, yields an apparent age spectrum (Fig. 8a) that can be interpreted in context of regional and local parameters available. The upper limit of 506±2Ma is interpreted as the likely maximum formation age of schistosity in this unit, however, this fabric may be even older. The age spectrum also records younger ages at c. 498-496 Ma that may reflect the influence of intrusion of the nearby boudinaged quartz-muscovite vein. The boudinaged quartz-muscovite vein itself yields a maximum intrusion age of c. 497 Ma from the muscovite age spectrum (Fig. 8c). This age spectrum also records ages at c. 493 Ma, which may reflect the effects of the later intruded undeformed quartz-muscovite vein. The three samples from this locality therefore appear to define a coherent set of events from schistosity formation by at least 506±2 Ma, intrusion of an initial phase of quartz-muscovite veining at c. 497 Ma, continued deformation, and finally intrusion of an undeformed quartz-muscovite vein at c. 493 Ma.

The likely maximum formation age of schistosity at c. 506 Ma agrees well with the timing of D_2 Delamerian episode (c. 505 Ma; Foden et al., 2006). Using Arrhenius data (Fig. 9b), the diffusion domains for muscovite

within the Tapanappa Schist began closing to argon diffusion at 352°C until final closure at 279°C. Such low closure temperatures could explain the preservation of very minor older age component in the schist. We interpret the interval of c. 4 My between the two veins at c. 497 Ma and c. 493 Ma as a period of

630 continued tectonic activity, possibly a regional fluid flow event. This could likely be a consequence of addition of heat into the crust, possibly due to prevailing extensional tectonics at the time as exemplified by the late-stage A-type granites and mafics in the region. The 493 Ma age marks the termination of deformation at the Kanmantoo Mine area.

635 In summary, the regional deformation fabric at the Kanmantoo Mine formed between c. 506-495 Ma based on the structural relationships and ages obtained from the host schist and quartz-muscovite vein, where the boudinaged vein truncates the two-mica schist no later than c. 495 Ma. Regional tectonics was active until the intrusion of non-boudinaged vein i.e., no later than c. 493 Ma.

640 Microstructure analyses are important in deciphering sequences of tectonic events in a region, principally the ones that have experienced a complex deformation history, and the Kanmantoo Mine area is one such example. Here, garnet growth is the last event to have occurred, justified by its static growth over the primary fabric in the schist (Fig. 6d-h). The presence of altered and pristine garnets hints towards their progressive growth during late syn- to post- Delamerian deformation. We observed the localisation of

645 garnets growing over or near cleavage domains while they rarely grow proximal to the microlithons (quartz-rich domains). During active orogenesis, fluid flow channelization is structurally controlled e.g., more fluid flow in deformed zones/rocks (Oliver, 1996). Along with this, the availability of reactant minerals exerts primary control on fluid-flow and reaction front propagation (Skelton et al., 1995; Kleine, 2015). Thus, growth of garnets is restricted to schistosity (mica-rich domains) due to the availability of 'reactant minerals' for

650 their formation relative to the microlithons. Such a mechanism is then more likely to alter and fracture the garnets in the vicinity of the schistosity relative to those growing in the microlithons. We approximate that garnet formation could relate to the circulation of hot-hydrothermal fluids in the area and associated evolving P-T conditions during retrogressed metamorphic period.

655 Flottmann et al., (1996) reported elevated concentration of MnO in the Tapanappa Formation schists, where enrichment is associated with exhalative fluids also evident through high MnO concentration of the garnets in this study (Supplement 4). It is probable that hydrothermal fluids in the area provided the necessary 'ingredients', concomitantly incorporating Mn concentrations from the host schist to form garnets at suitable P-T conditions. Our interpretation of $^{40}Ar/^{39}Ar$ data from the host schist estimates the interval of c.493-

660 487Ma as the period of garnet growth. Following this, exhumation of the schists may have destabilised the garnets forming secondary biotite as observed in our microstructures (Fig. 6g-h). This study has not attempted to precisely constrain the timing of garnet formation; therefore, this age estimate is rather relative.

Figure 10 is a time-space plot that represents our samples in relation to the established constraints.
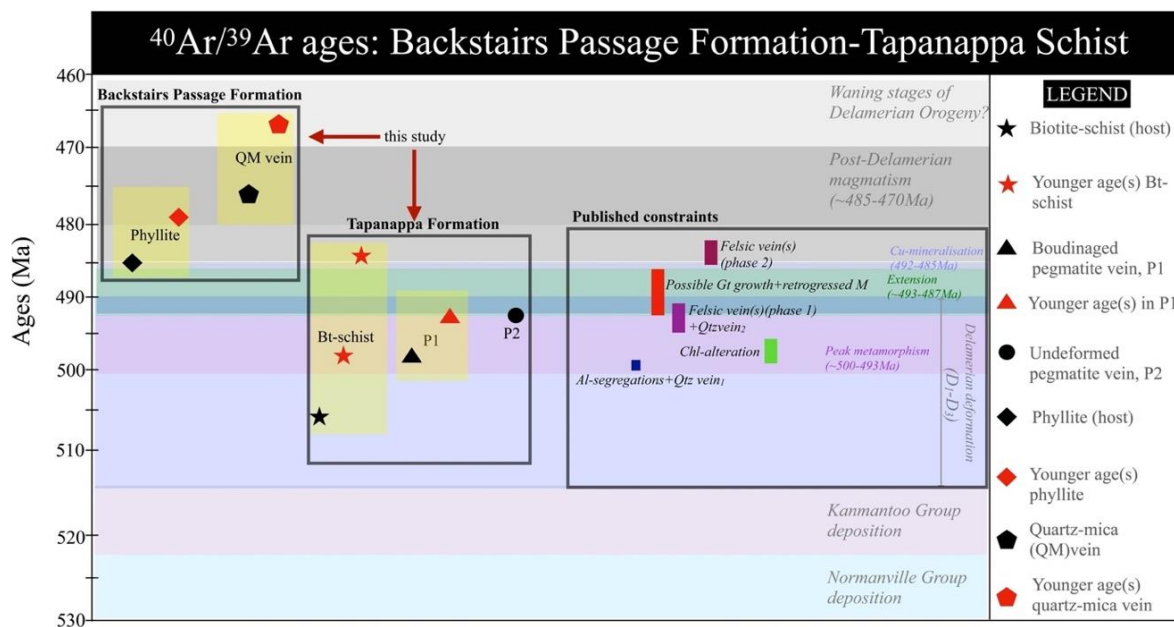
Figure 10. Time-space plot combining major geological episodes and results obtained from this study

The data obtained here has regional implications and agrees well with the established U-Pb, Rb/Sr and Sm-Nd ages reported in Turner et al, 1996; Foden et al., 2006; Foden et al., 2020. In addition to this, new age data with low uncertainty is reported. This paper highlights the complexity of dating and interpreting ^{40}Ar/^{39}Ar age results of micas from different stratigraphic units. Such age information is crucial for a region where geological episodes have occurred 1-2 My apart. In summary, the evidence of deformation events at Kanmantoo Mine area equate to the regional established D_2 and D_3 events are well observed in our ^{40}Ar/^{39}Ar age data.

6.3 Timing of regional and local tectonic events

Previous constraints on the timing of geological events that have occurred at the Kanmantoo Mine area lay the foundation for this study, however knowledge gaps remain. We have attempted to fit our results into the established sequence of events. Below is a visual representation of the simplified TSD (Fig. 11) for the Tapanappa Schist, compiling information on local and regional events, geochronology, and microstructural analyses.

(a) Established regional constraints

| Kanmantoo deposition c. 522-514Ma | Delamerian D₁ (c. 515Ma) | Delamerian D₂ (c. 505Ma) | Al segregations+Qtz vein₁ (c.498Ma) | Felsic veins₁+Quartz vein₂ (495-491Ma) | Delamerian D₃ (c. 490Ma) | Intrusion of felsic veins₂ (c.485-481Ma) | Extension+post-Delamerian intrusives (post c. 485Ma) |

Delamerian Deformation

Peak metamorphism (c.500-493Ma)

Cu mineralisation (c.492-485Ma)

Regional fluid flow (c.493-487Ma)

TSD (simplified)- this study, Tapanappa Formation

at least at c.498Ma

c. 498Ma   c. 485-481Ma c. 492-485Ma

>>>D>>>>

S_b S_p F Qtz_{veinB} P_B ΔAndΔSt S_z P_{NB} Qtz_{vein} Δ$Cu_{minerals}$
     S_{cren} ΔBt

c. 506Ma   c. 497Ma   c. 493Ma

● ⁴⁰Ar/³⁹Ar data, this study   ● Previous regional constraints
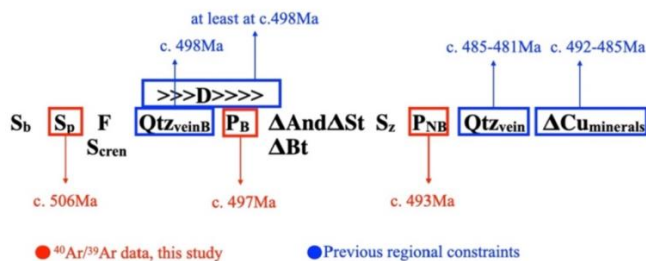
(b) Introduction of data from this study into existing regional constraints
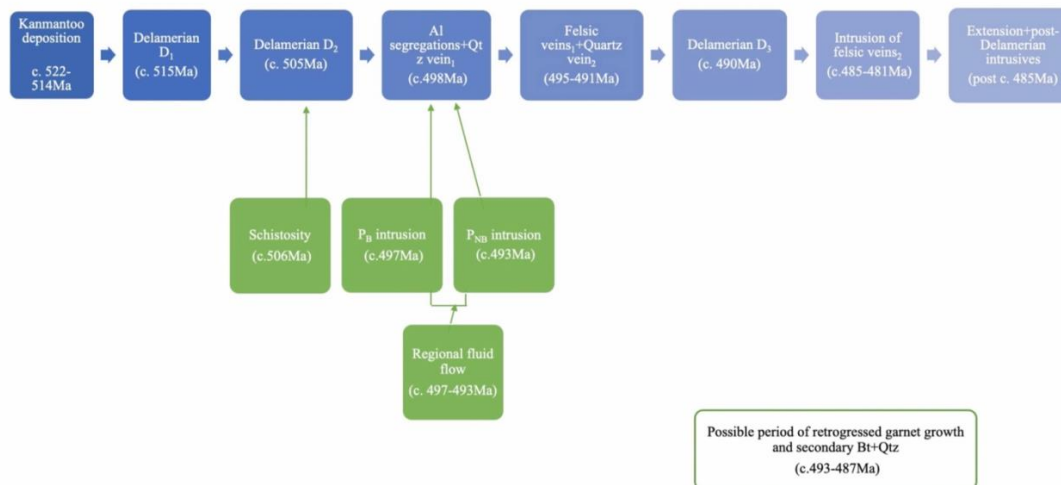
| Kanmantoo deposition c. 522-514Ma | Delamerian D₁ (c. 515Ma) | Delamerian D₂ (c. 505Ma) | Al segregations+Qtz vein₁ (c.498Ma) | Felsic veins₁+Quartz vein₂ (495-491Ma) | Delamerian D₃ (c. 490Ma) | Intrusion of felsic veins₂ (c.485-481Ma) | Extension+post-Delamerian intrusives (post c. 485Ma) |

Schistosity (c.506Ma) P_B intrusion (c.497Ma) P_{NB} intrusion (c.493Ma)

Regional fluid flow (c. 497-493Ma)

Possible period of retrogressed garnet growth and secondary Bt+Qtz (c.493-487Ma)

685
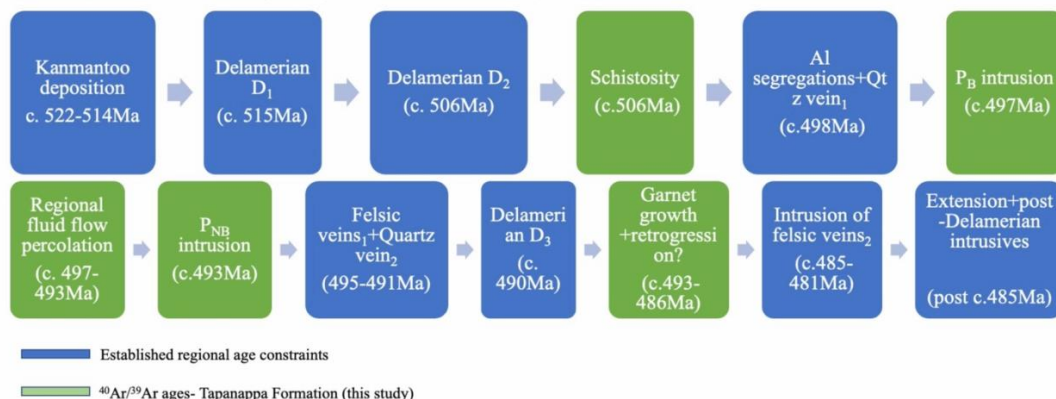
Figure 11. Compiled tectonic sequence diagram incorporating regional events and data from this study

6.4 Implications of younger ^{40}Ar/^{39}Ar ages in the stratigraphically older Backstairs Passage Formation

The Backstairs Passage Formation is stratigraphically older than the Tapanappa Formation, yet it has experienced lower grade metamorphism than the overlying Tapanappa Formation. Furthermore, the Backstairs Passage Formation records ages ranging from c. 484-481 Ma in the phyllite (sample 2746269, Fig. 7a), which are younger than the ages recorded in the Tapanappa Formation (sample 2746272, Fig. 8a).

The relationship between metamorphic grade, stratigraphic level and argon ages can be explained in two ways:

1. Based on Arrhenius plot analyses (Fig. 9), the host schist and phyllite have similar closure temperature ranges for the biotite-white mica composites dated in this study. As Tapanappa Formation overlies the Backstairs Passage Formation, it's early exhumation relative to the underlying Backstairs Passage Formation could explain the older Ar-ages preserved in the Tapanappa Formation. The Ar-diffusion systematics would have closed to diffusion earlier in the schist than in the underlying phyllite. Also, the higher ambient temperatures experienced by the phyllite would have kept it as an 'open-system' to argon diffusion for longer periods than the overlying schist.

2. The proximity of the Tapanappa Formation (schist) to the metamorphic core of the Delamerian Orogen at Reedy Creek than the Backstairs Passage Formation (phyllite) could explain the difference in the argon ages. The schist would have been affected earlier by the migmatisation event (c. 514 Ma, U-Pb zircon age Rathjen Gneiss as the source intrusive for migmatisation; Drexel and Preiss, 1995) hence recording older ages than the phyllite which was away from the metamorphic core. The dissipated heat from the migmatisation event would have reached the schist first and affected the phyllite later leading to mineral growth first in the schist (older ages) and later in the phyllite (younger ages).

The age range of c. 484-481 Ma observed in the Backstairs Passage Formation can be interpreted in two ways. The first way is to understand the S_{diff} fabric to have formed at least by c. 484 Ma followed by S_{cren} which formed at least by c. 481 Ma. The other interpretation is to consider the c. 484-481 Ma interval to bracket S_{cren} fabric formation only. Following this, the micaceous vein (sample 2746268) must have intruded the host after c. 476 Ma, with the age range in this sample from c. 476-468 Ma being younger than the youngest age of the mica from the phyllite host (c. 481 Ma).

In summary, S_{cren} had developed by c. 481 Ma and the cross-cutting quartz-muscovite vein intruded the phyllite between c. 476-468 Ma. The regional deformation affected the phyllite at Backstairs Passage Formation 10 My later than the Tapanappa Formation at the Kanmantoo Mine area. Deformation affecting

the phyllite lasted from at least c. 484 Ma to at most c. 468 Ma. The age data from this suggests that geological processes were operating in this part of the orogen ~10 My after the main period of Delamerian deformation conventionally reported (c. 514-490 Ma; Foden et al., 2006). We have attempted to fit our results into the established sequence of events. Below is a visual representation of the simplified TSD. A simplified TSD compiling age information from Backstairs Passage Formation and Tapanappa Formation together with published ages is presented in Fig. 12b.

Figure 12. Compiled tectonic sequence diagram incorporating regional events, Backstairs Passage and Tapanappa Formation

7 Conclusion

This study has attempted to the date the fabric forming minerals in the Backstairs Passage Formation and the Tapanappa Formation of the Cambrian Kanmantoo Group that has experienced deformation during the Delamerian Orogeny. The age(s) presented here broadly agree with the established ages of Delamerian deformation. The data presented from these stratigraphic units is restricted to these locations only and do not apply to the broader geological region affected by the Delamerian Orogeny.

The samples in this study were dated using $^{40}Ar/^{39}Ar$ geochronology employing temperature-controlled step-heating experiments. In summary, our analyses of the host two-mica schist from the Tapanappa Formation show the early mica fabric to have formed at least by c. 506 Ma, however, this fabric maybe older than this. The schist also records the effect of intrusion of a boudinaged vein at c. 495 Ma. The boudinaged vein (sample 2746270) at Kanmantoo Mine area records the effects of later undeformed (non-boudinaged) quartz-muscovite vein at c. 493 Ma closer to D_3 phase. Microstructure analyses of the schist indicates static garnet overgrowths on schistosity and a second generation of retrograde biotite forming at the expense of garnet. Using age information from the schist, we approximate the garnets to have formed at least by c. 487 Ma as a consequence of regional fluid-flow event exemplified by Cu-minerals observed in the region.

The younger ages of c. 484-481 Ma observed in the stratigraphically older Backstairs Passage Formation record the timing of fabric formation in this unit with two possible interpretations- either the main foliation formed at c. 484 Ma followed by crenulations forming at c. 481 Ma or the interval of c. 484-481 Ma brackets the formation of crenulation cleavage formation only. The micaceous quartz vein intruded the phyllite between c. 476-468Ma. The ages c. 484-468 Ma are younger than the conventional main interval of Delamerian deformation (c. 514-490 Ma) and are the new findings from this study.

These younger ages observed from the Backstairs Passage Formation within the Kanmantoo Group are suggestive of protracted periods of Delamerian deformation and its differentiated nature (effects not observed in the Tapanappa Formation) extending to as young as c. 468 Ma, in contrast to previous studies that have interpreted deformation to have ceased by c. 490 Ma.

Competing interests. The author has declared that there are no competing interests.

Acknowledgements. Mr. Shane Paxton is thanked for his guidance with mineral separation and sample preparation training. Dr. Arun Ojha is thanked for his assistance with insightful discussions and proof-reading of the manuscript. Dr. Anthony Reid and Dr. Geoff Fraser are thanked for their help with insightful discussions regarding the age data.

Financial support. This research forms part of a PhD project undertaken by the contact author from 2019-2023 and has been supported by the Mineral Exploration Cooperative Research Centre whose activities are funded by the Australian Government's Cooperative Research Centre Program. All samples were financially supported by the AuScope National Argon Map and the ANU Argon Lab.

References

Abbot, P., Burtt, A., Ferguson, D., and Moriarty, K.: Cambrian mineral resources come of age- the Kanmantoo revival. MESA Journal 36, 2005.

Arbon, H.: Bismuth distribution in the Cu-Au mineralisation of the Kanmantoo deposit, South Australia. Thesis, University of Adelaide, Australia, 2011.

Boger, S. D., and Miller, J. M.: Terminal suturing of Gondwana and the onset of the Ross–Delamerian Orogeny: the cause and effect of an Early Cambrian reconfiguration of plate motions. Earth and Planetary Science Letters, 219(1-2), 35-48, https://doi.org/10.1016/S0012-821X(03)00692-7, 2004.

Burtt, A. C., and Phillips, D.: Ar/Ar dating of a pegmatite, Kinchina Quarry, Murray Bridge, South Australia. MESA Journal 28, 2003.

Burtt, A. C., Abbott, P., and Fanning, M. C.: Definition of Teal Flat and Marne River volcanics and associated shear zone. Adelaide: Department of Primary Industries and Resources South Australia, Adelaide, 2000.

Drexel, J. F., and Preiss, W. V.: The geology of South Australia, Volume 2: The Phanerozoic: South Australia Geological Survey Bulletin. Geological Survey of South Australia, 1995.

Dymoke, P., & Sandiford, M.: Phase relationships in Buchan facies series pelitic assemblages: calculations with application to andalusite-staurolite para- geneses in the Mount Lofty Ranges, South Australia. Contributions to Mineralogy and Petrology, 110, 121-132, https://doi.org/10.1007/BF00310886, 1992.

Fanning, M. C.: Single grain dating of a granite sample from Cape Willoughby, Kangaroo Island. Prise Lab- oratories, Australian National University Progress Re- port 89-060. South Australia Department of Mines and Energy, Open File Envelope 8828, 1990.

Flottmann, T., Gum, J., and Haines, P.: Kanmantoo tectonics, sedimentology and metallogeny excursion field guide. Department of Mines and Energy, South Australia, 1996.

810 Flöttmann, T., Haines, P., Jago, J., James, P., Belperio, A., and Gum, J.: Formation and reactivation of the Cambrian Kanmantoo Trough, SE Australia: implications for early Palaeozoic tectonics at eastern Gondwana's plate margin. Journal of the Geological Society, London, 155, 525-539, https://doi.org/10.1144/gsjgs.155.3.0525, 1998.

815 Foden, J., Elburg, M. A., Dougherty-Page, J., and Burtt, A.: The Timing and Duration of the Delamerian Orogeny: Correlation with the Ross Orogen and Implications for Gondwana Assembly. The Journal of Geology, 114, 189-210, https://doi.org/10.1086/499570, 2006.

Foden, J., Elburg, M., Turner, S., Clark, C., Blades, M. L., Cox, G., . . . George, C.: Cambro-Ordovician magmatism in the Delamerian orogeny: Implications for tectonic development of the southern
820 Gondwanan margin. Gondwana Research, 81, 490-521, https://doi.org/10.1016/j.gr.2019.12.006, 2020.

Foden, J., Sandiford, M., Dougherty-Page, J., and Williams, I.: Geochemistry and geochronology of the Rathjen Gneiss: Implications for the early tectonic evolution of the Delamerian Orogen. Australian Journal of Earth Sciences, 46, 377-389, https://doi.org/10.1046/j.1440-0952.1999.00712.x, 1999.

825

Foden, J., Song, S., Turner, S., Elburg, M., Smith, P. B., Steldt, B., and Penglis, D. V.: Geochemical evolution of lithospheric mantle beneath S.E. South Australia. Chemical Geology, 182, 663-695, https://doi.org/10.1016/S0009-2541(01)00347-3, 2002.

830 Forster, M. A., and Lister, G. S.: Tectonic sequence diagrams and the structural evolution of schists and gneisses in multiply deformed terranes. Journal of the Geological Society, 165, 923-939, https://doi.org/10.1144/0016-76492007-016, August 2008.

Forster, M., and Lister, G.: Core-complex-related extension of the Aegean lithosphere initiated at the
835 Eocene-Oligocene transition. Journal of Geophysical Research: Solid Earth, 114(B2), https://doi.org/10.1029/2007JB005382, 2009.

Forster, M. A., and Lister, G. S.: Argon enters the retentive zone: reassessment of diffusion parameters for K-feldspar in the South Cyclades Shear Zone, Ios, Greece. Geological Society, London, Special
840 Publications, 332, 17-34, https://doi.org/10.1144/SP332.2, 2010.

Gibson, G. M., and Nihill, D. N.: Glenelg River Complex: western margin of the Lachlan Fold Belt or extension of the Delamerian Orogen into western Victoria? Tectonophysics, 214, 69-91, https://doi.org/10.1016/0040-1951(92)90191-8, 1992.

845

Gray, C. M., and Webb, J. A.: Provenance of Palaeozoic turbidites in the Lachlan Orogenic Belt: Strontium isotopic evidence. Australian Journal of Earth Sciences, 42(1), 95-105, https://doi.org/10.1080/08120099508728182, 1995.

850 Gray, D. R., Foster, D. A., Goscombe, B., Passchier, C. W., and Trouw, R. A.: ^{40}Ar/^{39}Ar thermochronology of the Pan-African Damara Orogen, Namibia, with implications for tectonothermal and geodynamic evolution. Precambrian Research, 150(1-2), 49-72, https://doi.org/10.1016/j.precamres.2006.07.003, 2006.

855 Gum, J. C.: The sedimentology, sequence stratigraphy and mineralisation of the Silverton Subgroup, South Australia. Adelaide: University of South Australia, Adelaide (unpubl.), 1998.

Haines, P. W., Jago, J. B., and Gum, J.: Turbidite deposition in the Cambrian Kanmantoo Group, South Australia. Australian Journal of Earth Sciences, 48, 465-478, https://doi.org/10.1046/j.1440-
860 0952.2001.00872.x, 2001.

Ireland, T., Morand, V. J., and Gibson, G.: Results from some recent SHRIMP U-Pb zircon dating of rocks from the Glenelg Zone of western Victoria. Geol. Surv. Vic. Tech. Rec. 2002/2, 2002.

865 Jago, J. B., Gum, J. C., Burtt, A. C., and Haines, P. W.: Stratigraphy of the Kanmantoo Group: a critical
element of the Adelaide Fold Belt and the Palaeo-Pacific plate margin, Eastern Gondwana. Australian
Journal of Earth Sciences, 50, 343-363, https://doi.org/10.1046/j.1440-0952.2003.00997.x, 2003.

Jenkins, R. J., and Sandiford, M.: Observations on the tectonic evolution of the southern Adelaide Fold
870 Belt. Tectonophysics, 214, 27-36, https://doi.org/10.1016/0040-1951(92)90188-C, 1992.

Jenkins, R. J., Cooper, J. C., and Compston, W.: Age and biostratigraphy of Early Cambrian tuffs from SE
Australia and southern China. Journal of the Geological Society, 159, 645-658,
https://doi.org/10.1144/0016-764901-127, 2002.
875

Kimpton, B. J.: The geological relationship between Kanmantoo Cu-Au deposit mineralisation,
hydrothermal metasomatism and igneous intrusives. Thesis, The University of Adelaide, 2018.

Kleine, B. I.: How do metamorphic fluids move through rocks? An investigation of timescales, infiltration
880 mechanisms and mineralogical controls. Stockholm: Stockholm University, 2015.

Lister, G. S., and Baldwin, S. L.: Modelling the effect of arbitrary PTt histories on argon diffusion in
minerals using the MacArgon program for the Apple Macintosh. Tectonophysics, 253(1-2), 83-109,
https://doi.org/10.1016/0040-1951(95)00059-3, 1996.
885

Lyons, N.: Evidence for magmatic hydrothermal mineralisation at Kanmantoo Copper deposit, South
Australia. Honours thesis, University of Adelaide, 2012.

Mancktelow, N. S.: The structure of the southern Adelaide Fold Belt, South Australia. In Jago, J. B., and
890 Moore, P. J., eds. The evolution of a Late Precambrian– Early Palaeozoic Rift Complex: the Adelaide
Geosyncline. Geological Society of Australia Special Publications, 16, 482-495, 1990.

Mauger, A., Keeling, J., Rolley, P., and Arbon , H.: Spectral analysis of drill core from the Kanmantoo
copper deposit. Geological Survey of South Australia, Department for Energy and Mining, Hillgrove
895 Resources, 2018.

Muston, J., Forster, M., Vasegh, D., Alderton, C., Crispin, S., and Lister, G.: Direct dating of overprinting
fluid systems in the Martabe epithermal gold deposit using highly retentive alunite. *Geochronology
Discussions*, *2021*, 1-31, https://doi.org/10.5194/gchron-5-153-2023, 2021.
900

Offler, R., and Fleming, P.: A synthesis of folding and metamorphism in the Mt. Lofty Ranges, South
Australia. Journal of Geological Society of Australia, 15, 245-266,
https://doi.org/10.1080/00167616808728697, 1968.

905 Oliver, N. H.: Review and classification of structural controls on fluid flow during regional metamorphism.
Journal of Metamorphic Geology, 14, 477-492, https://doi.org/10.1046/j.1525-1314.1996.00347.x, 1996.

Oliver, N. H., Dipple, G. M., Cartwright, I., and Schiller, J.: Fluid flow and metasomatism in the genesis of
the amphibolite-facies, pelite-hosted Kanmantoo Copper Deposit, South Australia. American Journal of
910 Science, 298, 181-218, https://doi.org/10.2475/ajs.298.3.181, 1998.

Parker, A. J.: Tectonic development and metallogeny of the Kanmantoo Trough in South Australia. Ore
Geology Reviews, 1, 203-212, https://doi.org/10.1016/0169-1368(86)90009-0, 1986.

915 Perkins, C., and Walsh, J. L.: Geochronology of the Mt. Read Volcanics, Tasmania, Australia. Economic
Geology, 88, 1176-1197, https://doi.org/10.2113/gsecongeo.88.5.1176, 1993.

Pollock, M. V., Spry, P. G., Tott, K. A., Koenig, A., Both, R. A., and Ogierman, J.: The origin of the
sediment-hosted Kanmantoo Cu-Au deposit, South Australia: Mineralogical considerations. Ore Geology
920 Reviews, 95, 94-117, 2018.

Preiss, W. V.: Early and Middle Palaeozoic Orogenesis: Delamerian Orogeny. In J. F. Drexel & W. V. Preiss (Eds.), The geology of South Australia. Vol. 2, The Phanerozoic, South Australia: Geological Survey, Bulletin 54, 45-57, 1995.

925

Reid, A., Forster, M., Preiss, W., Caruso, A., Curtis, S., Wise, T., ... and Lister, G.: Complex $^{40}Ar/^{39}Ar$ age spectra from low-grade metamorphic rocks: resolving the input of detrital and metamorphic components in a case study from the Delamerian Orogen. Geochronology, 4(2), 471-500, https://doi.org/10.5194/gchron-4-471-2022, 2022.

930

Renne, P. R., Balco, G., Ludwig, K. R., Mundil, R., and Min, K.: Response to the comment by WH Schwarz et al. on "Joint determination of ^{40}K decay constants and $^{40}Ar*/^{40}K$ for the Fish Canyon sanidine standard, and improved accuracy for $^{40}Ar/^{39}Ar$ geochronology" by PR Renne et. al. (2010). Geochimica et Cosmochimica Acta, 75(17), 5097-5100, https://doi.org/10.1016/j.gca.2010.06.017, 2011.

935

Rozendaal, A., Gresse, P. G., Scheepers, R., and Le Roux, J. P.: Neoproterozoic to Early Cambrian Crustal Evolution of the Pan-African Saldania Belt, South Africa. Precambrian Research, 97(3-4), 303-323, 138-146, https://doi.org/10.1016/S0301-9268(99)00036-4, 1999.

940 Rutherford, L., Hand, M., & Mawby, J.: Delamerian-aged metamorphism in the southern Curnamona Province, Australia: implications for the evolution of the Mesoproterozoic Olarian Orogeny. Terra Nova, 18(2), https://doi.org/10.1111/j.1365-3121.2006.00673.x, 21 March 2006.

Schiller, J. C.: Structural geology, metamorphism and origin of the Kanmantoo Copper deposit, South
945 Australia. Unpublished Ph.D. thesis, University of Adelaide, 2000.

Seccombe, P. K., Spry, P. G., Both, R. A., Jones, M. T., and Schiller, J. C.: Base Metal Mineralization in the Kanmantoo Group, South Australia: A Regional Sulfur Isotope Study. Economic Geology, 80, 1824-1841, https://doi.org/10.2113/gsecongeo.80.7.1824, 1985.

950

Skelton, A. D., Graham, C. M., and Bickle, M. J.: Lithological and Structural Controls on Regional 3-D Fluid Flow Patterns during Greenschist Facies Metamorphism of the Dalradian of the SW Scottish Highlands. Journal of Petrology, 36(2), 563-586, https://doi.org/10.1093/petrology/36.2.563, 1995.

955 Spell, T. L., and McDougall, I.: Characterization and calibration of $^{40}Ar/^{39}Ar$ dating standards. Chemical Geology, 198(3-4), 189-211, https://doi.org/10.1016/S0009-2541(03)00005-6, 2003.

Spry, P. G., Schiller, J. C., and Both, R. A.: Structure and metamorphic setting of base metal mineralisation in the Kanmantoo Group, South Australia. Proceedings of the Australasian Institute of
960 Mining and Metallurgy, 293, 57-65, 1998.

Thomson, B.P.: Kanmantoo Trough-regional geology and comments on mineralization. In: In: Knight, C.L. (Ed.), Economic Geology of Australia and Papua New Guinea, vol. 1. The Australasian Institute of Mining and Metallurgy, Melbourne, 555–560, 1975.

965

Toteff, S.: Cambrian sediment-hosted exhalative base metal mineralisation, Kanmantoo Trough, South Australia. Geol. Surv. S. Aust. Rep. Investig 57,41, 1999.

Turner, N. J., Black, L. P., and Kamperman, M.: Dating of Neoproterozoic and Cambrian orogenies in
970 Tasmania. Australian Journal of Earth Sciences, 45(5), 789-806, https://doi.org/10.1080/08120099808728433, 1998.

Turner, S. P., Foden, J. D., Sandiford, M., and Bruce, D.: Sm-Nd isotopic evidence for the provenance of sediments from the Adelaide fold belt and southeastern Australia with implications for episodic crustal
975 addition. Geochimica et Cosmochimica Acta, 57, 1837-1857, https://doi.org/10.1016/0016-7037(93)90116-E, 1993.

Turner, S. P., Kelley, S. P., VanderBerg, A. H., Foden, J. D., Sandiford, M., and Flöttmann, T.: Source of the Lachlan fold belt flysch linked to convective removal of the lithospheric mantle and rapid exhumation of the Delamerian-Ross fold belt. Geology, 24, 941-944, https://doi.org/10.1130/0091-7613(1996)024%3C0941:SOTLFB%3E2.3.CO;2, October 1996.

Wilson, G. L.: Structural setting and timing of the Kanmantoo Cu-Au deposit, Callington, SA. Adelaide: University of Adelaide, Australia, 2009.